



## Dynamic control of the high-affinity iron uptake complex in root epidermal cells

Amanda Martín Barranco, Julien Spielmann, Guillaume Dubeaux, Grégory Vert, Enric Zelazny

### ► To cite this version:

Amanda Martín Barranco, Julien Spielmann, Guillaume Dubeaux, Grégory Vert, Enric Zelazny. Dynamic control of the high-affinity iron uptake complex in root epidermal cells. *Plant Physiology*, 2020, 184 (3), pp.1236-1250. <10.1104/pp.20.00234>. <hal-02931857>

**HAL Id: hal-02931857**

**<https://hal.science/hal-02931857v1>**

Submitted on 17 Dec 2020

**HAL** is a multi-disciplinary open access archive for the deposit and dissemination of scientific research documents, whether they are published or not. The documents may come from teaching and research institutions in France or abroad, or from public or private research centers.

L'archive ouverte pluridisciplinaire **HAL**, est destinée au dépôt et à la diffusion de documents scientifiques de niveau recherche, publiés ou non, émanant des établissements d'enseignement et de recherche français ou étrangers, des laboratoires publics ou privés.



Distributed under a Creative Commons CC BY-NC-ND 4.0 - Attribution - Non-commercial use - No Derivative Works - International License

**Short title:** *Arabidopsis* iron uptake complex

# **Dynamic control of the high-affinity iron uptake complex in root epidermal cells**

Amanda Martín-Barranco<sup>1</sup>, Julien Spielmann<sup>2</sup>, Guillaume Dubeaux<sup>3</sup>, Grégory Vert<sup>2\*</sup>, and Enric Zelazny<sup>1,4\*</sup>

<sup>1</sup>Institute for Integrative Biology of the Cell (I2BC), UMR9198 CNRS/CEA/Univ. Paris Sud, Université Paris-Saclay, 91198 Gif-sur-Yvette, France.

<sup>2</sup>Plant Science Research Laboratory (LRSV), UMR5546 CNRS/University of Toulouse 3, 31320 Auzeville Tolosane, France.

<sup>3</sup>Division of Biological Sciences, Cell and Developmental Biology Section, University of California San Diego, La Jolla, CA 92093, USA.

<sup>4</sup>Current address: BPMP, CNRS, INRAE, Montpellier SupAgro, Univ Montpellier, 2 Place Viala, 34060 Montpellier Cedex 2, France.

\*Corresponding authors: Enric.Zelazny@supagro.fr ; Gregory.Vert@lrsv.ups-tlse.fr

The authors responsible for distribution of materials integral to the findings presented in this article in accordance with the policy described in the Instructions for Authors (www.plantphysiol.org) are: Enric Zelazny (Enric.Zelazny@supagro.fr) and Grégory Vert (Gregory.Vert@lrsv.ups-tlse.fr).

**Author contributions:** A.M.B., G.V. and E.Z. designed the research; A.M.B., J.S. and E.Z. performed the experiments; G.D. performed the quantification of co-localization and statistical analyses; A.M.B., J.S., G.D., G.V. and E.Z. analyzed data; A.M.B., G.V. and E.Z. wrote the manuscript.

30  
31  
32  
33  
34  
35  
36  
37  
38  
39  
40  
41  
42  
43  
44  
45  
46  
47  
48  
49  
50  
51  
52  
53  
54  
55

**Funding:** This work has benefited from a French State grant (reference ANR-10-LABX-0040-SPS, to E.Z.) managed by the French National Research Agency under an Investments for the Future program (reference n°ANR-11-IDEX-0003-02). This work was also funded by Marie Curie Actions (PCIG-GA-2012-334021, to G.V.), by the French National Research Agency (ANR-13-JSV2-0004-01, to G.V.) and the French Laboratory of Excellence project “TULIP” (ANR-10-LABX-41 and ANR-11-IDEX-0002-02 to G.V.). Guillaume Dubeaux is supported by an EMBO long-term postdoctoral fellowship (ALTF334-2018).

**One-sentence summary:** The three main actors of iron acquisition in *Arabidopsis* root, namely IRT1, FRO2, and AHA2, assemble into a dedicated protein complex.

## ABSTRACT

In plants, iron uptake from the soil is tightly regulated to ensure optimal growth and development. Iron absorption in *Arabidopsis* root epidermal cells requires the IRT1 transporter that also allows the entry of certain non-iron metals, such as Zn, Mn, and Co. Recent work demonstrated that IRT1 endocytosis and degradation are controlled by IRT1 non-iron metal substrates in an ubiquitin-dependent manner. To better understand how metal uptake is regulated, we identified IRT1-interacting proteins in *Arabidopsis* roots by mass spectrometry and established an interactome of IRT1. Interestingly, the AHA2 proton pump and the FRO2 reductase, both of which work in concert with IRT1 in the acidification-reduction-transport strategy of iron uptake, were part of this interactome. We confirmed that IRT1, FRO2, and AHA2 associate through co-immunopurification and split-ubiquitin analyses, and uncovered that they form tripartite direct interactions. We characterized the dynamics of the iron uptake complex and showed that FRO2 and AHA2 ubiquitination is independent of the non-iron metal substrates transported by IRT1. In addition, FRO2 and AHA2 are not largely endocytosed in response to non-iron metal excess, unlike IRT1. Indeed, we provide evidence that the phosphorylation of IRT1 in response to high levels of non-iron metals likely triggers dissociation of the complex. Overall, we propose that a dedicated iron-acquisition protein complex exists at the cell surface of *Arabidopsis* root epidermal cells to optimize iron uptake.

**Keywords:** IRT1, iron, *Arabidopsis*, transport, endocytosis, phosphorylation

86 **INTRODUCTION**

87         Iron is essential for plant growth and development as it plays fundamental roles in  
88 many cellular processes, including photosynthetic and respiratory electron transfer reactions.  
89 However, iron is also toxic when present in excess because it induces oxidative stress. Iron  
90 bioavailability to plants is often limited, such as in calcareous soils in which iron is present in  
91 the form of insoluble complexes (Briat et al., 2015). Iron is a limiting factor for plant biomass  
92 production and hence is required as an important component of agriculture productivity. To  
93 maintain iron homeostasis, plants must tightly regulate iron absorption from the soil. In non-  
94 graminaceous plants, including the model plant *Arabidopsis thaliana*, iron absorption by root  
95 epidermal cells is achieved through the so-called strategy I, which requires three successive  
96 steps. Firstly, soil ferric chelates are solubilized by local rhizosphere acidification via the  
97 release of protons by the proton pump  $H^+$ -ATPase2 (AHA2). Solubilized  $Fe^{3+}$  ions are then  
98 reduced to  $Fe^{2+}$  by the Ferric Reduction Oxydase2 (FRO2) reductase and finally transported  
99 into the cell by the iron transporter Iron Regulated Transporter1 (IRT1) (Palmer and Guerinot,  
100 2009; Thomine and Vert, 2013; Jeong et al., 2017). During this acidification-reduction-  
101 transport mechanism, reduction of  $Fe^{3+}$  ions by FRO2 has been proposed to be the rate-  
102 limiting step in iron acquisition (Robinson et al., 1999; Connolly et al., 2003). In *Arabidopsis*,  
103 the expression of *IRT1*, *FRO2*, and *AHA2* genes is activated under iron-limited conditions  
104 through the direct action of the basic Helix-Loop-Helix (bHLH) transcription factor FER-like  
105 Iron Deficiency-Induced Transcription Factor (FIT) that can form heterodimers with other  
106 bHLH proteins (Colangelo and Guerinot, 2004; Jakoby et al., 2004; Yuan et al., 2008). Apart  
107 from the predominant role of IRT1, FRO2, and AHA2, another membrane protein called  
108 ATP-Binding Cassette G37 (ABCG37/PDR9) was demonstrated to be involved in  
109 *Arabidopsis* iron acquisition by exporting coumarins in the rhizosphere under iron deficiency  
110 (Fourcroy et al., 2014). These excreted phenolic compounds chelate  $Fe^{3+}$  and facilitate iron  
111 availability for reduction by FRO2 (Fourcroy et al., 2016). Similar to the other components of  
112 the *Arabidopsis* iron-acquisition machinery, the *ABCG37/PDR9* gene is transcriptionally  
113 induced in response to iron deficiency in a FIT-dependent manner (Rodriguez-Celma et al.,  
114 2013).

115         IRT1 is a major player in the regulation of plant iron homeostasis, as attested by the  
116 severe chlorosis and the lethality of the *irt1-1* knock-out mutant (Vert et al., 2002).  
117 Interestingly IRT1 is a broad-spectrum transporter, which also allows the absorption of metals

such as zinc, manganese, cobalt, and cadmium, in addition to iron (Rogers et al., 2000; Vert et al., 2001; Vert et al., 2002). The dynamics of IRT1 protein and its role in the maintenance of metal homeostasis in *Arabidopsis* have been widely investigated. IRT1 localizes to early endosomes in root epidermal cells and rapidly cycles between this compartment and the cell surface to perform iron absorption (Barberon et al., 2011). Importantly, IRT1 dynamics requires clathrin-mediated endocytosis and is controlled by ubiquitination on two cytosol-exposed lysine residues (Barberon et al., 2011), a process mediated by the E3 ubiquitin ligase IRT1 DEGRADATION FACTOR1 (IDF1) (Shin et al., 2013; Dubeaux et al., 2018). Surprisingly, IRT1 ubiquitination and endocytosis are not regulated by iron, the primary substrate of the IRT1 transporter, but rather by its secondary metal substrates (Zn, Mn, and Co, herein called non-iron metal substrates). These non-iron metal substrates, which are highly reactive and toxic when present in excess in plant cells, were recently demonstrated to regulate IRT1 endocytosis (Barberon et al., 2014). In the presence of physiologically relevant concentrations of non-iron metal substrates, a functional IRT1-mCitrine fusion protein is localized in early endosomes and to some extent at the plasma membrane of root epidermal cells. Interestingly, in the presence of an excess of non-iron metal substrates, IRT1-mCitrine is targeted to late endosomes and then reaches the vacuole for degradation, whereas it is exclusively localized to the plasma membrane in the absence of such metals. The sensing of the excess of non-iron metal substrates is directly mediated by IRT1 through the binding of metals on a histidine-rich stretch located in IRT1 large cytosolic loop (Dubeaux et al., 2018). Hence, IRT1 was proposed to act as a transceptor, combining transporter and receptor properties (Cointy and Vert, 2019). Non-iron metal binding to IRT1 allows the recruitment of Calcineurin B-like (CBL)-interacting serine/threonine-protein kinase 23 (CIPK23) and subsequent phosphorylation of IRT1. This in turn allows the lysine-63 polyubiquitination of IRT1 by IDF1, triggering IRT1 endocytosis and targeting to the vacuole (Dubeaux et al., 2018). The control of IRT1 degradation by its secondary substrates certainly constitutes a protective mechanism allowing limitation of the absorption of readily available  $\text{Zn}^{2+}$ ,  $\text{Mn}^{2+}$ , and  $\text{Co}^{2+}$  ions that, contrary to  $\text{Fe}^{3+}$ , do not need prior reduction by FRO2 to be transported (Zelazny et al., 2011). Interestingly, the plasma membrane pool of IRT1 is present at the outer polar domain of root epidermal cells, which is necessary for proper radial transport of metals in the root (Barberon et al., 2014). IRT1 physically interacts with FYVE1, a protein recruited to the Endosomal Sorting Complexes Required for Transport (ESCRT) in late endosomes (Barberon et al., 2014; Gao et al., 2014). FYVE1 drives the maintenance of IRT1 lateral polarity, through a mechanism that is not fully understood. Interference with *FYVE1*

expression induces apolar localization of IRT1 at the plasma membrane and disturbs metal uptake in *Arabidopsis* (Barberon et al., 2014). IRT1 recycling from endosomes to the plasma membrane was shown to require Sorting Nexin 1 (SNX1) (Ivanov et al., 2014). Recently, the peripheral membrane protein ENHANCED BENDING1 (EHB1) was demonstrated to interact with IRT1 in a calcium-dependent manner and was proposed to act as an inhibitor of IRT1-mediated iron transport (Khan et al., 2019).

Since IRT1 is an essential determinant of root metal uptake in low-iron conditions, we sought to identify additional proteins involved in IRT1 dynamics/activity or working in concert with IRT1 to better characterize how plant metal homeostasis is controlled. Using co-immunopurification (co-IP) of IRT1 and identification of IRT1-interacting proteins by mass spectrometry, we shed light on the existence of a dedicated protein complex composed of IRT1, FRO2, and AHA2 that likely optimizes iron uptake in root epidermal cells. We also uncovered that IRT1 is selectively removed from the complex in response to non-iron metal excess, in a process involving its phosphorylation.

## RESULTS

### IRT1 interactome in *Arabidopsis* root epidermal cells

To better understand how the non-iron metal-mediated internalization of IRT1 is controlled in root epidermal cells, we searched for proteins interacting with IRT1 upon non-iron metal excess. To this purpose, a functional IRT1-mCitrine fusion protein expressed under the control of the *IRT1* promoter in *Arabidopsis irt1-1* null mutant (Dubeaux et al., 2018) was immunopurified, and co-purified proteins were identified by mass spectrometry. *irt1-1*/IRT1::IRT1-mCitrine transgenic line and *Ws* wild-type (WT) plants, used as a negative control, were initially grown for nine days on MS/2 medium containing iron, transferred for five days onto a medium lacking iron and containing physiological concentrations of non-iron metals to induce IRT1-mCitrine expression, and finally transferred to a medium without iron and containing an excess of non-iron metal substrate for two days. To purify the transmembrane IRT1-mCitrine protein, root protein extracts from IRT1-mCitrine-expressing plants were solubilized with a soft non-ionic detergent, n-Dodecyl  $\beta$ -D-maltoside (DDM), to preserve the interactions between IRT1 and its partners. Then, IRT1-mCitrine and the associated proteins were immunopurified with anti-GFP antibodies coupled to magnetic microbeads, the same procedure was performed on DDM-solubilized proteins from WT plant

184 roots. Immunopurified proteins from IRT1-mCitrine and WT plants were separated by SDS-  
185 PAGE (Supplemental Fig. 1) and analyzed by mass spectrometry. Proteins were considered as  
186 interacting with IRT1 when specifically identified in IRT1-mCitrine immunopurified fraction  
187 with at least two different peptides. This approach allowed the identification of 142 putative  
188 IRT1 interactants (Supplemental Dataset 1). Among these, 31 were found in the two  
189 independent experiments whereas 111 were detected in only one of the two replicates. Since  
190 the control of IRT1 trafficking is of the utmost importance for the regulation of this  
191 transporter, we specifically looked for IRT1-interacting proteins that are linked to the  
192 secretory or endocytic pathways (Table1). Clathrin was found as putatively interacting with  
193 IRT1, which is in accordance with our previous results showing that IRT1 undergoes clathrin-  
194 mediated endocytosis (Barberon et al., 2011; Barberon et al., 2014). Interestingly SEC13a and  
195 SEC31b proteins were identified as IRT1 putative interactants, suggesting a role of coat  
196 protein complex II (COPII) machinery in the export of IRT1 from the endoplasmic reticulum  
197 (ER) to the Golgi apparatus (Chung et al., 2016). Conversely, IRT1 probably also undergoes  
198 retrograde transport from the Golgi to the ER since it interacts with components of COPI  
199 vesicles (Table 1) (Yorimitsu et al., 2014). Another interesting group of IRT1 interactants are  
200 proteins linked to *Arabidopsis* metal homeostasis such as the Pleiotropic drug resistance 8 /  
201 Penetration 3 protein that was proposed to act as a cadmium extrusion pump (Kim et al.,  
202 2007) (Table 1). IRT1 also associates with two iron transporters from the VIT family;  
203 however, the relevance of this interaction remains unclear since these proteins were described  
204 as localizing to the ER body membrane (Yamada et al., 2013). Recently, rhizosphere-excreted  
205 coumarins were shown to be important for iron acquisition in an IRT1-dependent manner  
206 (Fourcroy et al., 2016). Interestingly, the Feruloyl-Coenzyme A 6'-Hydroxylase 1 (F6'H1)  
207 (Schmid et al., 2014) and the Cytochrome P450/CYP82C4 (Rajniak et al., 2018), which are  
208 both involved in coumarin biosynthesis, were identified as putative IRT1-interacting proteins  
209 (Table 1). In addition, FRO2 and AHA2, which are known to both act in concert with IRT1 in  
210 the acidification-reduction-transport strategy for iron uptake in *Arabidopsis thaliana*, were  
211 also identified (Table 1). Mass spectrometry analyses performed on IRT1 co-immunopurified  
212 fractions indeed identified peptides specific to the AHA2 isoform, but also identified peptides  
213 common to AHA2 and other AHA proteins, mostly AHA1. However, since no peptide  
214 specific to other AHA proteins than AHA2 were found, and because rhizosphere acidification  
215 is chiefly mediated by AHA2 in lack of iron (Santi and Schmidt, 2009), we decided to focus  
216 our attention on AHA2. These observations indicate that IRT1, FRO2, and AHA2 likely  
217 associate to drive iron uptake. To gain further insight into the regulation of the iron uptake



machinery, we characterized in more detail the interaction and the spatial organization of the three major actors of iron acquisition, namely FRO2, AHA2, and IRT1.

### **IRT1 directly interacts with FRO2 and AHA2**

To validate the observations obtained from mass spectrometry analyses, the interactions between IRT1 and AHA2/FRO2 were first investigated in *Arabidopsis* roots by performing co-IP combined with immunodetections. We analyzed the interaction between IRT1-mCitrine, expressed under the control of *IRT1* promoter, and endogenous AHA2 protein by using a previously described antibody raised against Plasma Membrane H<sup>+</sup>-ATPase 2 (PMA2) from *Nicotiana plumbaginifolia* that recognizes AHA2 and also other *Arabidopsis* AHA proteins. When IRT1-mCitrine IP fraction was probed with anti-PMA2 antibodies, a strong signal corresponding to the expected size of AHA2 (104 kDa) was detected, whereas no signal was observed in the IP fraction from WT plant roots used as a negative control (Fig. 1A). Although this signal may correspond in part to other AHA isoforms than AHA2 due to a lack of specificity of the anti-PMA2 antibodies, this result suggests that endogenous AHA2 likely associates with IRT1 in root epidermal cells. The existence of an IRT1-AHA2 complex is substantiated by other protein-protein interaction assays described hereafter. Since no antibody raised against FRO2 was available, we generated a translational fusion of FRO2 expressed under control of the *FRO2* promoter in the previously described *fro2* mutant named *frd1-1* (Robinson et al., 1999). Expression of FRO2 fused at its N-terminal end to the mCherry fluorescent protein (mCherry-FRO2) complemented the hypersensitivity of *frd1-1* to low iron, even for transgenic lines expressing low levels of mCherry-FRO2 (Supplemental Fig. 2A and B). This clearly shows that mCherry-FRO2 fusion protein is fully functional. Consistently, mCherry-FRO2 protein was only detected in root epidermal cells (Supplemental Fig. 2C), highlighting the specificity of *FRO2* promoter, as previously reported (Connolly et al., 2003). To analyze the interaction between FRO2 and IRT1 in *Arabidopsis* roots by co-IP, we generated transgenic lines co-expressing mCherry-FRO2 and IRT1-mCitrine under control of the *FRO2* and *IRT1* promoters, respectively. Transgenic lines co-expressing IRT1-mCitrine and RabD1-mCherry, the latter co-localizing with IRT1 in endosomes (Supplemental Fig. 3), were used as a negative control. mCherry-FRO2 was co-immunopurified with IRT1-mCitrine whereas RABD1-mCherry was not, proving that FRO2 and IRT1 form a protein complex in root epidermal cells (Fig. 1B and Supplemental Fig. 4).

The interaction between IRT1 and AHA2/FRO2 was also confirmed by a split-ubiquitin assay, which allows the detection of direct interactions between membrane proteins in yeast. Such an approach has been successfully implemented with IRT1 and IDF1 (Shin et al., 2013; Dubeaux et al., 2018). IRT1 fused to the mutated N-terminal half of ubiquitin (NubG), which is unable to spontaneously reassemble with the C-terminal part of ubiquitin (Cub), was co-expressed in yeast with AHA2 or FRO2 fused to Cub linked to the chimeric transcription factor ProteinA-LexA-VP16 (PLV) (Fig. 1C). Physical interactions between IRT1 and AHA2/FRO2 were tested through the ability to rescue yeast growth on a selective medium. Yeast co-expressing NubG-IRT1 with AHA2-Cub or FRO2-Cub grew on a selective medium, similarly to the respective positive controls expressing NubWT with AHA2-Cub/FRO2-Cub. However, no growth was observed for the respective negative controls expressing NubG with AHA2-Cub/FRO2-Cub. As an additional negative control for split-ubiquitin, NubG-IRT1 was co-expressed with an unrelated transmembrane protein, specifically the brassinosteroid receptor BRI1, fused to Cub. Whereas yeast co-expressing NubWT with BRI1-Cub (positive control of interaction) grew on a selective medium, no growth was observed when BRI1 and IRT1 were co-expressed, indicating that these two proteins do not interact. Interestingly, our split-ubiquitin assay also revealed that AHA2 and FRO2 could physically associate with each other (Fig. 1C). This result was confirmed in plants by co-IP approaches showing that endogenous AHA2 is co-immunopurified with mCherry-FRO2 from *Arabidopsis* root protein extracts (Supplemental Fig. 5). Altogether, these observations validate the existence of a protein complex in root epidermal cells that gathers the different actors of the high-affinity iron uptake machinery in close proximity.

### Differential regulation of the iron uptake system by ubiquitination

We recently demonstrated that IRT1 endocytosis is controlled by the non-iron metal substrates of IRT1 (Dubeaux et al., 2018). Upon an excess of these metals, IRT1 ubiquitination strongly increases leading to the endocytosis and the degradation of IRT1 in the vacuole. Interestingly, proteomic analyses allowed the identification of AHA2 and FRO2 as part of the *Arabidopsis* ubiquitinome (Kim et al., 2013; Johnson and Vert, 2016; Walton et al., 2016). Since AHA2 and FRO2 belong to an IRT1-containing protein complex, we wondered whether ubiquitination of these proteins could be co-regulated by non-iron metal availability. First, we analyzed the ubiquitination profile of AHA2 and FRO2 by performing

IP of AHA2-GFP and mCherry-FRO2 expressed in *Arabidopsis* roots, followed by the immunodetection of ubiquitination with the P4D1 general anti-ubiquitin antibodies. In the presence of physiological concentrations of non-iron metal substrates, AHA2-GFP and mCherry-FRO2 IP fractions probed with P4D1 antibodies exhibited high-molecular-weight smears that are typical of ubiquitinated proteins as observed for IRT1-mCitrine used as a control (Fig. 2). To quantify the effect of non-iron metal regime on the ubiquitination of the investigated proteins, the signal intensity observed for the anti-ubiquitin immunoblots performed on IRT1-mCitrine, AHA2-GFP, or mCherry-FRO2 immunopurified proteins was measured and normalized to the corresponding immunopurified proteins (Fig. 2C). As previously observed (Dubeaux et al., 2018), a short treatment with an excess of non-iron metals led to a strong increase in IRT1-mCitrine ubiquitination (Fig. 2A and C). By contrast, the pool of ubiquitinated AHA2-GFP and mCherry-FRO2 remained unchanged in both metal regimes (Fig. 2A, B and C, and Supplemental Fig. 6). Hence, although AHA2, FRO2, and IRT1 belong to the same complex involved in a common mechanism i.e. iron acquisition, ubiquitination of these proteins is differentially regulated by metal availability.

### **Selective endocytosis of IRT1 in response to non-iron metal excess**

Although the intracellular dynamics of IRT1 and AHA2 were previously independently investigated (Barberon et al., 2011; Dubeaux et al., 2018; Haruta et al., 2018), the subcellular distribution of FRO2 has not previously been determined. Thus, the respective localization of IRT1-mCitrine and FRO2/AHA2 expressed as mCherry fusion proteins was investigated. We used root-tip epidermal cells as i) these cells are well suited to analyze the precise localization of endocytosed plasma membrane proteins and ii) the metal-triggered endocytosis of IRT1 was already characterized in such cells (Dubeaux et al., 2018). Interestingly, in the absence of iron and in the presence of physiologically relevant amounts of non-iron metal substrates, mCherry-FRO2 was present at the plasma membrane in the outer polar domain facing the rhizosphere, as observed for IRT1-mCitrine (Fig. 3A, left panel) (Barberon et al., 2014; Dubeaux et al., 2018). FRO2 also co-localized with IRT1 in intracellular vesicles (Mander's coefficient,  $M2 = 0.48$ ) (Fig. 3A, left panel and 3C), which correspond to early endosomes since IRT1 constitutes a marker of these compartments in such metal conditions (Barberon et al., 2011; Dubeaux et al., 2018). In contrast to IRT1 and FRO2, AHA2-mCherry displayed an apolar plasma membrane localization in epidermal cells

in the same metal conditions and although AHA2-mCherry was observed in a limited number of endosomes, these were mostly co-labeled with IRT1-mCitrine ( $M2 = 0.39$ ) (Fig. 3B, left panel and 3D).

The intracellular dynamics of FRO2 and AHA2 were then investigated after a short-term treatment with an excess of non-iron metal substrates that triggers IRT1 endocytosis and its subsequent degradation (Dubeaux et al., 2018). Upon non-iron metal excess, IRT1-mCitrine was depleted from the cell surface and accumulated in late endosomes (Fig. 3A and 3B, left panels). mCherry-FRO2 and AHA2-mCherry were, however, mostly detected at the plasma membrane, even though they were also found to co-localize with IRT1-mCitrine in late endosomes (Fig. 3A and 3B, left panels). To quantify the response to metals, the ratio of plasma membrane to intracellular fluorescence signal intensities was measured for the three fusion proteins under physiological non-iron metal provision or in the presence of an excess of these metals (Fig. 3A and 3B, right panels). As previously reported, the plasma membrane/intracellular ratio highly decreased for IRT1-mCitrine in response to non-iron metal excess (Dubeaux et al., 2018). For mCherry-FRO2 and AHA2-mCherry, however, no significant difference was observed, indicating that FRO2 and AHA2 are not largely endocytosed in response to non-iron metal excess. However, the level of co-localization of FRO2 and IRT1 in endosomes significantly increased with non-iron metal excess ( $M2 = 0.69$ ) compared to control conditions ( $M2 = 0.48$ ) (Fig. 3C), suggesting a minor effect of non-iron metal status on FRO2 endocytosis. On the other hand, the co-localization level between AHA2 and IRT1 in endosomes was not significantly modified by non-iron metal substrates (Fig. 3D).

The absence of a massive internalization of FRO2 and AHA2 in response to non-iron metal excess suggests that the IRT1/FRO2/AHA2 complex dissociates prior to IRT1 endocytosis. Since the phosphorylation of residues in the large cytosolic loop of IRT1 was shown to be the trigger of IRT1 ubiquitin-dependent endocytosis upon non-iron metal substrate excess (Dubeaux et al., 2018), we investigated whether phosphomimic (IRT1<sub>S/TxD</sub>) or non-phosphorylatable (IRT1<sub>S/TxA</sub>) variants of IRT1 would display modified association with AHA2 and FRO2. Using split-ubiquitin approaches, we observed that yeast co-expressing NubG-IRT1<sub>S/TxD</sub> and AHA2- or FRO2-Cub grew slower on the selective medium than yeast co-expressing NubG-IRT1 or NubG-IRT1<sub>S/TxA</sub> together with AHA2- or FRO2-Cub (Fig. 4A, B). To better quantify the effect of the respective IRT1 variants, we measured yeast growth in liquid cultures. We consistently observed reduced growth for yeast co-expressing

FRO2 or AHA2 with IRT1<sub>S/TxD</sub> compared to their wild-type or IRT1<sub>S/TxA</sub> counterparts (Fig. 4C, D), although NubG-IRT1<sub>S/TxD</sub> protein accumulated to the same extent as wild-type or IRT1<sub>S/TxA</sub> when expressed in yeast cells (Supplemental Fig. 7). These results show that the phosphomimic variant of IRT1 displays a reduced interaction with AHA2 and FRO2. Altogether, these observations clearly indicate a role for IRT1 phosphorylation in dissociation of the high-affinity iron uptake complex upon non-iron metal excess.

## DISCUSSION

### IRT1 interactome: new insight into IRT1 dynamics and metal uptake

IRT1 mediates the absorption of iron but also non-iron metal substrates such as Zn, Mn, and Co in root epidermal cells and is a major actor of metal nutrition in *Arabidopsis*. Previous studies revealed that the tight control of IRT1 intracellular dynamics by IDF1, CIPK23, FYVE1, or SNX1 is essential to maintain metal homeostasis and to ensure optimal plant growth and development (Shin et al., 2013; Barberon et al., 2014; Ivanov et al., 2014; Dubeaux et al., 2018). To better understand how IRT1 is controlled in the cell, we searched for further IRT1-interacting proteins by performing IP of the functional IRT1-mCitrine fusion protein expressed under the control of *IRT1* promoter coupled to mass spectrometry analyses. Co-IP has the great advantage to reveal physiologically relevant protein-protein interactions in plant cells and regarding false positives, co-IP does not generate more than the yeast two-hybrid or the split-ubiquitin techniques and results in less than using bimolecular fluorescence complementation (BiFC) (Xing et al., 2016). Besides, co-IP was successfully used in the past to identify interactants of channels and receptors (Karlova et al., 2006; Bellati et al., 2016). One must consider that an interactome provides an overview of proteins putatively interacting with a bait, but that each candidate protein has to be validated by an independent protein-protein interaction technic before further investigation to avoid putative artifacts. Here, we decided to (i) use the *IRT1* endogenous promoter to maximize the detection of interactions between IRT1 and its interactants in relevant cell types, i.e. root epidermal cells, and (ii) validate each candidate of interest using the split-ubiquitin technic. Two independent co-IP/mass spectrometry experiments were performed, which provides qualitative data on proteins interacting with IRT1. Using another replicate would have certainly allowed us to obtain more quantitative data. Besides, since several very interesting candidates such as FRO2 were identified in one of the two experiments, we decided to include the proteins that were identified in only one replicate in the IRT1 interactome. Among 142 proteins putatively

interacting with IRT1, a group of proteins related to intracellular trafficking emerged, which included clathrin, tubulin, and actin (Table 1). An association between clathrin and IRT1 is in agreement with the previously reported clathrin-mediated internalization of IRT1 from the plasma membrane (Barberon et al., 2014). The co-IP approach does not allow the determination of whether two proteins directly interact or not; however, according to what is known for other cargo proteins, it is likely that the interaction between IRT1 and clathrin is mediated by an unknown adaptor protein. So far the role of actin and tubulin in IRT1 dynamics is poorly understood; however, since these proteins are known to be involved in plant endocytosis (Fan et al., 2015), their presence in the IRT1-interactome also opens interesting perspectives. Two small G proteins from the Rab class, namely RAB GTPase homolog A1D and RAB GTPase homolog 1C, were also identified as putative interactants of IRT1 (Table 1). Although the role of these two proteins in intracellular trafficking is still elusive, similar Rab proteins were described to act in plant endocytic pathways (Qi and Zheng, 2013). Intriguingly, the IDF1 E3 ubiquitin ligase and the CIPK23 kinase that are important for IRT1 endocytosis and were demonstrated to interact with IRT1 in split-ubiquitin and yeast-two hybrid candidate approaches, respectively (Shin et al., 2013; Dubeaux et al., 2018), were not co-purified with IRT1 in the present study. Given the functions of IDF1 and CIPK23, their interactions with IRT1 are probably very transient and may be lost during the co-IP procedure contrary to other systems such as split-ubiquitin and yeast-two hybrid where these associations would be stabilized (Xing et al., 2016). Until now, studies of IRT1 trafficking in plant cells mainly described endocytic mechanisms including IRT1 internalization from the plasma membrane in an ubiquitin-dependent process or IRT1 recycling from endosomes to the plasma membrane. How IRT1 traffics along the secretory pathway to reach the plasma membrane remains largely unknown, even though *Malus xiaojinesis* IRT1 was proposed to exit the ER in COPII vesicles (Tan et al., 2018). The *Arabidopsis* IRT1 interactome provides interesting clues on these aspects since IRT1 was found to putatively interact with several components of the COPII machinery that is sequentially recruited to the surface of the ER membrane to induce the formation of transport vesicles and ensure the delivery of cargo proteins to the Golgi apparatus (Chung et al., 2016) (Table 1). Membrane proteins exit the ER via the recognition of specific cytoplasmic export motifs by the COPII machinery; these signals include diacidic motifs corresponding to (D/E)x(D/E), with x representing any amino acid residue (Zelazny et al., 2009). A diacidic motif (EDD) located in the large cytosolic loop of IRT1 at the position 180 may be involved

in the packaging of IRT1 in COPII vesicles and its export from the ER, although this remains to be experimentally determined.

Besides the IRT1 interactants linked to intracellular trafficking, proteins involved in metal homeostasis represent a very interesting group of candidates (Table 1). Recently, coumarins, which are excreted in the rhizosphere by PDR9, were demonstrated to be important for *Arabidopsis* iron acquisition by chelating  $\text{Fe}^{3+}$  and as a result facilitating iron availability for FRO2 (Fourcroy et al., 2014; Fourcroy et al., 2016). Intriguingly, IRT1 potentially interacts with F6'H1 and Cytochrome P450/CYP82C4 that are both involved in coumarin biosynthesis (Schmid et al., 2014; Rajniak et al., 2018), but the meaning of these interactions remains unclear, notably because PDR9 was not identified as interacting with IRT1. However, solubilization of this large transmembrane protein may not be optimal in the conditions we used for the co-IP and other approaches will be necessary to determine whether PDR9 and IRT1 could work in concert among a common protein complex. Interestingly, FRO2 and AHA2, which act with IRT1 in the acidification-reduction-transport strategy for iron acquisition, were found to interact with IRT1.

### **IRT1, FRO2, and AHA2 form an iron-acquisition complex to optimize iron uptake in *Arabidopsis* roots**

By combining co-IP analyses and split-ubiquitin assays, we showed that IRT1 associates with FRO2 and AHA2 proteins, but also that FRO2 and AHA2 interact together (Fig. 1). Importantly, the tripartite physical interactions between IRT1, FRO2, and AHA2 are direct, suggesting the existence of a dedicated protein complex at the cell surface for iron uptake. Interaction between IRT1 and FRO2/AHA2 is probably not required for the intrinsic activity of IRT1, since heterologous expression of IRT1 alone allows phenotypic complementation of the *fet3 fet4* yeast mutant defective in iron uptake (Eide et al., 1996). Similar to IRT1, FRO2 was also observed at the outer polar domain of the plasma membrane in epidermal cells from the root tip (Fig. 3) and from the differentiated zone of the root (Supplemental Fig. 8A). The co-polarity between FRO2 and IRT1 proteins in this domain of the plasma membrane highlights the specificity of their functions achieved at the interface between the root surface and the rhizosphere. On the other hand, AHA2 distribution in the plasma membrane of root epidermal cells was homogenous (Fig. 3 and Supplemental Fig. 8B), suggesting that AHA2 does not obligatory associate with FRO2 and IRT1. This result is in accordance with AHA2 function not being restricted to iron acquisition (Yuan et al., 2017;

Hoffmann et al., 2018; Pacifici et al., 2018). Even though the performed interaction tests do not provide any information on the localization of the IRT1/FRO2/AHA2 complex, co-localization analyses suggest that IRT1 may interact with FRO2 and AHA2 in the plasma membrane and in endosomes (Fig. 3 and Supplemental Fig. 8). In the future, Förster resonance energy transfer-fluorescence lifetime imaging microscopy (FRET-FLIM), which allows the detection of protein-protein interactions in living plant cells with a high spatial and temporal resolution (Zelazny et al., 2007), may reveal where IRT1 interact with FRO2 and AHA2 in the cell.

IRT1 intracellular dynamics is regulated by ubiquitination notably in response to an excess of non-iron metal substrates, following which IRT1 ubiquitination is enhanced, thus triggering its endocytosis and degradation in the vacuole (Dubeaux et al., 2018). Our biochemical analyses revealed that FRO2 and AHA2 are also ubiquitinated; however, their ubiquitination is not modulated by the non-iron metal provision (Fig. 2 and Supplemental Fig.6). This is consistent with the endocytosis of both proteins being rather constitutive and not regulated by non-iron metals (Fig. 3). In this context, the ubiquitination of FRO2 and AHA2 appears to be involved in a non-degradative process. First, FRO2 and AHA2 may undergo mono-ubiquitination that is known to promote internalization from the cell surface but to be insufficient for vacuolar targeting (Lauwers et al., 2010). Second, the internalized pool of AHA2 and FRO2 may be rapidly de-ubiquitinated in endosomes allowing their recycling to the plasma membrane. Third, since ubiquitination is not only involved in endocytosis and degradation but is also implicated in other processes such as the allosteric regulation of proteins (Komander, 2009), we may speculate that FRO2 and AHA2 ubiquitination may convey this type of regulation. Although the identity of the E3 ubiquitin ligase at stake is unknown, IDFI represents a possible candidate for constitutive ubiquitination of AHA2 and FRO2 that will have to be tested in the future. The fact that AHA2 and FRO2 likely carry out other functions independent of iron nutrition may provide an explanation for their not being degraded upon non-iron metal excess. Indeed, AHA2 was previously reported to contribute to acidic growth or phosphorus uptake (Yuan et al., 2017; Hoffmann et al., 2018; Pacifici et al., 2018). FRO2 may play a role in copper reduction since *frd1-1* mutants lack low iron-inducible copper chelate reductase activity and 35S::FRO2 plants display elevated copper reduction (Yi and Guerinot, 1996; Robinson et al., 1999; Connolly et al., 2003). The absence of internalization of FRO2 and AHA2 from the plasma membrane in root epidermal cells in response to non-iron metal excess indicates that the



IRT1/FRO2/AHA2 complex must disassemble prior to IRT1 endocytosis to release AHA2 and FRO2 pools that may engage in other processes. In response to non-iron metal excess, IRT1 is phosphorylated by CIPK23 in its large cytosolic loop, boosting the interaction with the E3 ubiquitin ligase IDF1 and yielding polyubiquitinated IRT1 (Dubeaux et al., 2018). We demonstrated in the present study that phosphorylation of IRT1 at the same residues also controls the disassembly of the root high-affinity iron uptake complex (Fig. 4). Phosphorylation of IRT1 therefore has two opposite effects: dissociation of the IRT1/AHA2/FRO2 complex and recruitment of IDF1. Although phosphorylation is often considered as a post-translational modification allowing the recruitment of downstream factors, there is mounting evidence that it also controls the disassembly of protein complexes (Zhang et al., 2010; Couto et al., 2016). The fact that AHA2 and FRO2 were identified in our co-IP/mass spectrometry analysis as interacting with IRT1 in non-iron metal excess is rather surprising, since IRT1 phosphorylation in response to non-iron metal excess induces the dissociation of the IRT1/FRO2/AHA2 complex. However, this may not induce total dissociation of the complex, as evidenced by the residual interaction observed between the phosphomimic IRT1 and AHA2/FRO2. This is also supported by the partial co-localization of FRO2 and AHA2 with IRT1 in late endosomes under non-iron metal excess. In addition, we showed that the level of co-localization between FRO2 and IRT1 in late endosomes slightly increased with non-iron metal excess, suggesting that a small proportion of FRO2 is still able to associate with IRT1 in these conditions. Therefore, our co-IP/mass spectrometry analysis carried out when plants experience non-iron metal excess likely allowed us to identify the small pool of FRO2 and AHA2 still interacting with IRT1 in endosomes. This may explain why a limited number of FRO2 peptides were identified by proteomics.

The biological significance of iron uptake using a specific platform at the cell surface is unclear but likely relies in the chemistry of iron. Although iron is abundant in most soils, its bioavailability to plants is often limited. This is especially true for calcareous soils, which represent one third of cultivated lands, where iron is present under the form of insoluble complexes (Briat et al., 2015). During the iron-acquisition process, rhizosphere acidification by the root is essential to increase iron availability, indeed the solubility of iron increases 1000-fold for every one unit drop in pH (Olsen et al., 1981). However, this acidification process, mainly mediated by AHA2 under iron deficiency (Santi and Schmidt, 2009), is very local, which likely impacts on the efficiency of iron uptake. Moreover, the presence of oxygen in most soils likely provokes the rapid reoxidation of  $\text{Fe}^{2+}$  produced by FRO2 into

Fe<sup>3+</sup> that is not transported by IRT1. Thus, we propose that the tripartite protein complex gathering IRT1, FRO2, and AHA2 together creates a local environment of pH and Fe<sup>2+</sup> concentration in the rhizosphere that favors an optimal acquisition of iron (Fig. 4E). To experimentally validate this model, mutated versions of these proteins that do not interact with each other but that conserve their activities need to be generated to evaluate the functional outcome on iron uptake. However, this requires deep knowledge about the structure or interaction domains between these highly hydrophobic membrane proteins, which is currently missing. Alternatively to the local environment theory, we can also speculate that reduced iron is directly transferred from FRO2 to IRT1 by a channeling mechanism, similar to what has been described for metabolic pathways. Channeling consists in the transfer of the product of a proximal activity as substrate to a distal activity without equilibration with bulk solvent, which increases the efficiency of the kinetic process (Kwok et al., 2006). Such mechanism requires the close proximity of the donor and acceptor sites. Interestingly, channeling of iron was described in yeast between the multicopper oxidase Fet3p, which oxidizes Fe<sup>2+</sup> to Fe<sup>3+</sup>, and the iron permease Ftr1p that transports Fe<sup>3+</sup> into the cells, with both proteins forming a hetero-oligomeric complex (Kwok et al., 2006; Singh et al., 2006). Further work will elucidate whether FRO2 and IRT1 use a similar mechanism. Whether the formation of an iron-acquisition complex comprising IRT1, FRO2, and AHA2 is conserved in plants other than *Arabidopsis* remains to be determined. This complex is probably not present in rice (*Oryza sativa*) that combines two strategies to take up iron from the soil: a phytosiderophore-based system allowing the acquisition of Fe<sup>3+</sup> (Inoue et al., 2009; Lee et al., 2009) and the use of Fe<sup>2+</sup> transporters such as OsIRT1 (Ishimaru et al., 2006). Indeed, Fe<sup>3+</sup> chelate reductase activity has been shown to not be required for Fe<sup>2+</sup> uptake under iron deficiency in rice, suggesting that OsIRT1 works independently of OsFRO2-like proteins (Ishimaru et al., 2006). In paddy fields, where rice plants are grown, Fe<sup>2+</sup> is abundant due to the low redox potential and therefore rice plants do not need to reduce Fe<sup>3+</sup> to Fe<sup>2+</sup> (Ishimaru et al., 2007). So far, the description of protein complexes aimed at optimizing nutrient uptake in plant remains scarce. To our knowledge, only the interaction between glutamine synthase, the principal ammonia assimilatory enzyme, and the aquaglyceroporin Nodulin 26, a transporter of NH<sub>3</sub>, was proposed to promote efficient assimilation of nitrogen in soybean (Masalkar et al., 2010). Although experimental evidence is still needed, the co-localization between FRO2/AHA2 and IRT1 in early endosomes in the presence of physiologically relevant levels of non-iron metals suggests that the iron-acquisition complex may exist in this compartment in addition to the plasma membrane (Fig.4E). This complex may help plant metal uptake by translocating iron

from endocytic vesicles to the cytosol. Alternatively, the AHA2/FRO2/IRT1 complex may simply cycle between early endosomes and the plasma membrane in a constitutive manner or in response to some undetermined stimulus. Finally, since early endosomes/trans-Golgi network constitute a crossroad between endocytic and secretory pathways in plants (Dettmer et al., 2006), the presence of the IRT1/FRO2/AHA2 complex in early endosomes may also reflect a step in the delivery of a pre-formed complex to the plasma membrane. Future work will be needed to discriminate between these different scenarios.

## MATERIAL AND METHODS

### Plant material and growth conditions

*Arabidopsis thaliana* wild-type (WT) plants (Col-0, Col-gl1, and Ws), the *fro2* loss-of-function mutant named *frd1-1* (Robinson et al., 1999), the previously described *irt1-1/IRT1::IRT1-mCitrine* line (Dubeaux et al., 2018), and the various transgenic plants generated in this study were vertically grown in sterile conditions at 21°C with 16 h light/8 h dark cycles with a light intensity of 90  $\mu\text{mol m}^{-2} \text{s}^{-1}$  using Philips 17W F17T8/TL741 bulbs. The plant growth medium used was half-strength Murashige and Skoog (MS/2) medium containing 1% sucrose (w/v), 1% (w/v) agar, and various concentrations of metals. Hence, depending on the experiment (see below), plants were grown in the absence of iron and in the presence of physiological concentrations of IRT1 secondary substrates Zn (15  $\mu\text{M}$ ), Mn (50  $\mu\text{M}$ ), and Co (0.05  $\mu\text{M}$ ) (-Fe +Metals) or in the presence of 10-fold more Zn, Mn, and Co (-Fe +++Metals) corresponding to an excess of non-iron metal substrates, as previously described (Dubeaux et al., 2018). Plants have also been grown in iron-replete conditions using MS/2 medium containing 50  $\mu\text{M}$  or 100  $\mu\text{M}$  Fe-EDTA (+Fe).

For immunopurifications followed by mass spectrometry analyses, *irt1-1/IRT1::IRT1-mCitrine* transgenic lines and Ws WT plants were initially grown for 9 days on MS/2 medium containing 50  $\mu\text{M}$  Fe-EDTA, transferred for 5 days onto a -Fe +Metals medium to induce IRT1-mCitrine expression, and finally subjected to a -Fe +++Metals treatment for 48 h. To confirm the interactions between IRT1, FRO2, and AHA2 by co-immunopurifications, the various genotypes were grown for 11 days on MS/2 medium containing 50  $\mu\text{M}$  Fe-EDTA, and then transferred for 4 days on a -Fe +Metals medium supplemented with 300  $\mu\text{M}$  of the iron chelator Ferrozine [3-(2-pyridyl)-5,6-diphenyl-1,2,4-triazine sulfonate] to ensure a rapid and strong expression of genes under the control of *IRT1* and *FRO2* promoters.

To analyze mCherry-FRO2, AHA2-GFP, and IRT1-mCitrine ubiquitination profiles, the appropriate transgenic lines as well as WT plants used as negative controls were grown for 11 days on -Fe +Metals MS/2 solid medium. Then, plants were transferred for 2 h in -Fe +Metals (control) or -Fe +++Metals MS/2 liquid medium as previously described (Dubeaux et al., 2018).

For microscopy analyses, transgenic lines expressing IRT1/AHA2/FRO2 fusion proteins under the control of *IRT1* promoter, were first grown for 11 days on a -Fe +Metals MS/2 medium to ensure protein expression. Then, before observation, plants were transferred for 2 h in -Fe +Metals (control) or -Fe +++Metals MS/2 liquid medium. The localization of mCherry-FRO2 protein in *frd1-1*/FRO2::mCherry-FRO2 transgenic lines was performed on plants grown for 11 days in -Fe +Metals condition.

For mCherry-FRO2 functionality test, *frd1-1*/FRO2::mCherry-FRO2 transgenic lines, *frd1-1* mutant, and Col-gl1 WT plants were grown for 11 days on MS/2 lacking iron (-Fe +Metals) or on MS/2 supplemented with 100  $\mu$ M Fe-EDTA (control conditions). Roots from iron-starved transgenic lines and *frd1-1* (negative control) were collected to analyze mCherry-FRO2 protein accumulation by Western blot analysis as detailed below.

### Constructions and generation of *Arabidopsis* transgenic lines

All the constructions described in this section were obtained using the MultiSite Gateway® Three-Fragment Vector Construction system. The *FRO2* promoter corresponding to a sequence of 1,845 bp upstream of the *FRO2* start codon was amplified from *Arabidopsis thaliana* genomic DNA using the attB4.promoFRO2 forward and attB1r.promoFRO2 reverse primers (supplemental Table 1) and subsequently cloned into the pDONR.P4P1R entry vector. The *FRO2* open reading frame (ORF) was amplified from *Arabidopsis* cDNAs with the attB2r.FRO2 forward and attB3.FRO2 reverse primers (supplemental Table 1) and cloned into the pDONR.P2RP3 entry vector. The *AHA2* ORF without the stop codon was amplified from *Arabidopsis* cDNA with the AHA2.F forward and AHA2.R reverse primers and was cloned into the pDONR.221 entry vector. The mCherry sequence without stop codon was amplified with attB1.mCherry forward and attB2.mCherry reverse primers and also cloned into the pDONR.221 entry vector (supplemental Table 1). Entry vectors carrying the *IRT1* and *35S* promoters (pDONR.P4P1R-IRT1 and pDONR.P4P1R-35S) or the GFP and the mCherry coding sequence allowing C-terminal fusions (pDONR.P2RP3-GFP and

pDONR.P2RP3-mCherry) were previously described (Marques-Bueno et al., 2016; Dubeaux et al., 2018). Final destination vectors for expression in plants were obtained by multisite Gateway® recombination using the entry vectors described above and the pH7m34GW and pK7 m34GW destinations vectors used for mCherry and GFP fusions, respectively. The following constructs were generated: FRO2::mCherry-FRO2, IRT1::mCherry-FRO2, IRT1::AHA2-mCherry, and 35S::AHA2-GFP.

The previously described *irt1-1*/IRT1::IRT1-mCitrine line (Dubeaux et al., 2018) was transformed with FRO2::mCherry-FRO2, IRT1::mCherry-FRO2, and IRT1::AHA2-mCherry constructions by the floral-dipping technique using *Agrobacterium tumefaciens*. The *frd1-1* mutant and Col-0 plants were transformed with the FRO2::mCherry-FRO2 and 35S::AHA2-GFP constructs, respectively. The *irt1-1*/IRT1::IRT1-mCitrine transgenic line was crossed with the Wave marker line number 25 expressing RabD1-mCherry fusion protein under the control of UBQ10 promoter (Geldner et al., 2009).

## Immunopurifications

Immunopurifications (IP) were performed on approximately 500 mg of *Arabidopsis* roots, mostly as previously described (Dubeaux et al., 2018). Briefly, for IRT1-mCitrine IP followed by mass spectrometry, for co-IP analyses between IRT1-mCitrine and mCherry-FRO2, as well as for co-IP analyses between mCherry-FRO2 and endogenous AHA2, roots were ground in liquid nitrogen and resuspended in IRT1 solubilization buffer (50 mM Tris-HCl (pH 7.4), 150 mM NaCl, 5 mM EDTA, 1% (w/v) n-Dodecyl  $\beta$ -D-maltoside (DDM), and plant-specific protease inhibitors (Sigma-Aldrich)). For co-IP analyses between IRT1-mCitrine and endogenous AHA2, roots were ground and resuspended in RIPA buffer (50 mM Tris-HCl (pH 7.5), 150 mM NaCl, 0.5% (w/v) sodium deoxycholate, 1% (v/v) IGEPAL®CA-630, 0.1% (w/v) SDS, and plant-specific protease inhibitors (Sigma-Aldrich)). After two successive centrifugations at  $3,800 \times g$  for 10 min at 4°C, the resultant supernatants were collected and solubilization of membrane proteins was continued for 1 h 30 min at 4°C on a rotating wheel. Samples were then centrifuged at  $100,000 \times g$  for 1 h at 4°C to remove unsolubilized material and supernatants containing solubilized proteins were recovered for IPs. This ultracentrifugation step avoids the immuno-capture of proteins present in patches of residual non-solubilized membranes, allowing the IP to be carried out on solubilized protein complexes only. IPs of GFP and mCitrine fusion proteins were performed using  $\mu$ MACS GFP isolation kit (Miltenyi Biotec) whereas IP of mCherry fusion proteins was performed using

RFP-Trap®\_MA magnetic beads (Chromotek), following the instructions of the manufacturers. Before elution, extensive washes were performed with IRT1 solubilization buffer or RIPA buffer depending on the IP type. Co-IP analyses followed by mass spectrometry were performed twice. Co-IP combined with immunodetections were performed thrice with similar results.

To analyze the ubiquitination profile of AHA2-GFP and IRT1-mCitrine, the solubilization of fusion proteins as well as the IP procedure were performed exactly as previously described (Dubeaux et al., 2018). The same protocol was used for mCherry-FRO2 except that the protein was immunopurified with RFP-Trap®\_MA magnetic beads (Chromotek). Three independent analyses of ubiquitination profiles were performed.

### **Mass spectrometry analysis**

For sample preparation, proteins from each eluate were separated by SDS-PAGE in order to fractionate the protein samples into two fractions, including proteins 10–63 kDa and above 63 kDa, respectively, to exclude abundant contaminating IRT1-mCitrine protein at 63 kDa. After Coomassie-Blue staining, each gel fraction was cut into bands and subjected to in-gel trypsin digestion with the Progest robot (Genomic Solutions) using standard conditions including reduction and alkylation as described previously (Blanchet et al., 2014). Tryptic peptides extracted from the different bands of each gel fraction were pooled, vacuum dried, and resuspended in 0.1% (v/v) formic acid prior to nanoLC-MS/MS mass spectrometry analyzes. The same cutting pattern of the SDS-PAGE lane was performed for each eluate.

Tryptic peptides from the two or three SDS-PAGE fractions from each eluate were analyzed separately by nanoLC-MS/MS with the Triple-TOF 4600 mass spectrometer (ABSciex) coupled to the nanoRSLC ultra performance liquid chromatography (UPLC) system (Thermo Scientific) equipped with a trap column (Acclaim PepMap100C18, 75  $\mu$ m i.d.  $\times$  2 cm, 3  $\mu$ m) and an analytical column (Acclaim PepMapRSLCC18, 75  $\mu$ m i.d.  $\times$  50 cm, 2  $\mu$ m, 100 Å). Peptides were loaded at 5  $\mu$ l/min with 0.05% (v/v) TFA in 5% (v/v) acetonitrile and peptide separation was performed at a flow rate of 300 nl/min with a 5–35% (v/v) solvent B gradient in 40 min. Solvent A was 0.1% (v/v) formic acid in water, and solvent B was 0.1% (v/v) formic acid in 100% acetonitrile. NanoLC-MS/MS experiments were conducted in a Data Dependent acquisition method by selecting the 20 most intense precursors for CID fragmentation with Q1 quadrupole set at low resolution for better sensitivity.

Protein identification was performed by processing raw data with MS Data Converter software (AB Sciex) for generating .mgf data files and protein identification were performed using the MASCOT search engine (Matrix science, London, UK) against the Swissprot and TAIR10 databases with carbamidomethylation of cysteines set as fixed modification and oxidation of methionines as variable modifications. Peptide and fragment tolerance were set at 20 ppm and 0.05 Da, respectively. Results were analyzed with Scaffold 3.6.5 software (Proteome Software). Proteins were validated when identified with at least two unique peptides and 95% probability levels for both peptides and proteins.

### **Extraction of total proteins and immunoblots**

Total proteins were extracted from around 100 mg of *Arabidopsis* roots ground in liquid nitrogen and directly resuspended in 2X SDS sample buffer. Samples were heated at 65°C for 10 min, centrifuged 10 min at  $20,000 \times g$  and finally supernatants were collected and directly used for SDS-PAGE. Protein extraction from yeast was carried out as previously described (von der Haar, 2007).

Immunoblot analyses were performed as previously described (Barberon et al., 2011). Immunodetection of GFP and mCitrine fusion proteins was performed using an anti-GFP antibody conjugated to horseradish peroxidase (HRP) (Miltenyi Biotec 130-091-833, 1/5,000). mCherry fusion proteins were monitored with a rabbit anti-DsRed antibody (Clontech 632496, 1/5,000). Endogenous AHA2 protein was immunodetected using a rabbit antibody initially raised against the Plasma Membrane H<sup>+</sup>-ATPase 2 (PMA2) from *Nicotiana glauca* (W1C) diluted 1/15,000 (Morsomme et al., 1998). Ubiquitin modifications were detected with the P4D1 mouse anti-ubiquitin antibody (Millipore 05-944, 1/4,000). The detection of NubG-IRT1 protein from yeast used anti-HA antibodies (Miltenyi Biotec 130-091-972, 1/7,000). Anti-tubulin antibodies were used as loading control (Agrisera AS10 681, 1/5,000). The anti-rabbit IgG or anti-mouse IgG secondary antibodies coupled to HRP were both diluted 1/20,000. Detection of HRP chemiluminescence was performed using SuperSignal West Dura Extended Duration Substrate (Thermo Scientific) in a Chemidoc Touch Imaging system (Bio-Rad). Stain-Free protein staining (Bio-Rad) was used as a loading control as previously described (Dubeaux et al., 2018). To quantify IRT1-mCitrine, AHA2-GFP, and mCherry-FRO2 ubiquitination levels under different metal regimes, signal intensity observed with anti-ubiquitin immunoblots performed on IRT1-mCitrine, AHA2-

GFP, or mCherry-FRO2 immunopurified proteins was measured using Image Lab 6.0.1 and normalized to the quantity of immunopurified proteins detected in IP with anti-GFP or anti-DsRed antibodies. To facilitate comparisons, the ubiquitination level measured in the presence of physiological concentrations of non-iron metal substrates was arbitrary fixed to 1.

## **Constructions and split-ubiquitin assay**

Split-ubiquitin vectors were generated using the Gateway® technology. First, the *FRO2* ORF without the stop codon and the *AHA2* ORF with the stop codon were amplified with *FRO2.F/FRO2.R* and *AHA2.F/AHA2stop.R* primers, respectively (supplemental Table 1), and were both cloned into the pDONR.221 entry vector. pDONR.221-BRI1 without stop was previously generated (Martins et al., 2015) and pDONR.221-AHA2 without stop was created in this study as mentioned above. Then, *FRO2*, *AHA2*, and *BRI1* ORFs without the stop codon were inserted into pMetYC-DEST destination vector (Hachez et al., 2014) to produce methionine-repressible constructs *FRO2*-Cub-PLV, *AHA2*-Cub-PLV, and *BRI1*-Cub-PLV, respectively, where Cub corresponds to the C-terminal part of ubiquitin and PLV to a chimeric transcription factor. *AHA2* ORF with the stop codon was cloned into the pNX35-DEST destination vector to generate the NubG-AHA2 fusion wherein NubG corresponds to the mutated N-terminal part of ubiquitin. The NubG-IRT1, NubG-IRT1<sub>S/TxD</sub>, and NubG-IRT1<sub>S/TxA</sub> constructs were previously described (Dubeaux et al., 2018). It is important to note that NubG and Cub were fused to a cytosolic part of IRT1, *FRO2*, *AHA2*, and *BRI1*, according to the known or predicted topology of these proteins. The wild-type ubiquitin N-terminal fragment (NubWT) expressed by the pNubWT-Xgate vector and the NubG fragment expressed by the non-recombined pNX35-DEST vector were used as a positive and negative control, respectively (Hachez et al., 2014).

Split-ubiquitin assay was performed as previously described (Dubeaux et al., 2018). Briefly, THY.AP4 yeast strain was co-transformed with the Nub and Cub constructs of interest and co-transformed cells were selected on SD medium lacking Leu and Trp. Then, yeast co-expressing Cub-PLV fusion proteins with NubG fusion proteins or NubG (negative control of interaction) or NubWT (positive control of interaction) were dropped in serial dilutions (O.D. 1, 0.1, 0.01) onto SD medium without Leu and Trp (control medium) or onto SD medium lacking Leu, Trp, His, Ade (selective medium) supplemented with 500 µM methionine (250 µM methionine for IRT1/BRI1 interaction test) to limit the expression of the Cub-PLV fusion



proteins. Yeast growth on control and selective medium was recorded after 24 h and 48 h at 30°C, respectively. Besides internal negative interaction tests performed by co-expressing Cub-PLV fusion proteins with NubG, co-expression of NubG-IRT1 and BRI1-Cub-PLV was used as an additional negative control. Quantification of interactions were carried out using liquid yeast cultures and by measuring O.D. over time. Three independent split-ubiquitin interaction tests were performed with similar results.

### **Confocal microscopy**

Microscopy was performed with a Leica SP8 upright confocal laser scanning microscope. For mCitrine and mCherry imaging, the 514-nm and 561-nm lasers were used, respectively. Before observation, plants were mounted in MS/2 liquid medium containing the proper metal composition (-Fe +Metals or -Fe +++ Metals). Representative images are shown. For quantifications, z-stacks encompassing the whole cell volume were imaged and then subjected to maximum projection. The Mander's coefficient (M2) of mCherry-FRO2 and AHA2-mCherry endosomal structures showing overlap with IRT1-mCitrine labeled endosomes were determined using the ImageJ plugin Coloc2. 27 cells (3 independent cells from 3 different plants among 3 independent experiments) were analyzed for each condition and genotype. The M2 coefficient is the ratio of the summed intensities of pixels from the red image, for which the intensity in the green channel is above zero, to the total intensity in the red channel. M2 coefficients vary from 0 to 1, the former value corresponding to non-overlapping endosomes and the latter reflecting 100% co-localization between both channels. A ratio of 0.5 indicates a 50% overlap between the two channels. Here, we used M2 to reflect the co-localization between mCherry-FRO2 and IRT1-mCitrine, or AHA2-mCherry and IRT1-mCitrine. An unpaired *t*-test was used to determine whether the overlapping was different in response to metal excess (-Fe +++Metals). The ratios of plasma membrane over intracellular signal content were obtained by selecting whole-cell and intracellular content mean fluorescence with ImageJ.

### **Statistical analyses**

For confocal microscopy experiments, a representative image is shown. Statistical analyses were performed using the software GraphPad Prism 7. The sample size and statistical tests used are mentioned in the figure legends.

766  
767  
768  
769  
770  
771  
772  
773  
774  
775  
776  
777  
778  
779  
780  
781  
782  
783  
784  
785  
786  
787  
788  
789  
790  
791  
792  
793  
794  
795  
796  
797

## **Accession numbers**

Sequence data from this article can be found in the GenBank/EMBL data libraries under accession numbers: *IRT1* (AT4G19690), *FRO2* (AT1G01580), *AHA2* (AT4G30190), and *BRI1* (AT4G39400).

## **Supplemental Data**

**Supplemental Figure S1.** Immunopurification of IRT1-mCitrine and the associated proteins.

**Supplemental Figure S2.** Expression of mCherry-FRO2 complements the *frd1-1* mutant phenotype in iron-deficient conditions.

**Supplemental Figure S3.** IRT1-mCitrine and RabD1-mCherry co-localize in early endosomes in *Arabidopsis* root epidermal cells.

**Supplemental Figure S4.** mCherry-FRO2 protein is not cross-immunopurified with anti-GFP antibody.

**Supplemental Figure S5.** FRO2 and AHA2 interact in *Arabidopsis* root cells.

**Supplemental Figure S6.** FRO2 and AHA2 are ubiquitinated in *Arabidopsis* root cells in a metal-independent manner, replicate.

**Supplemental Figure S7.** Phosphomimic and non-phosphorylatable mutations in IRT1 do not influence IRT1 protein accumulation in yeast.

**Supplemental Figure S8.** Co-localization of IRT1 and FRO2/AHA2 in differentiated root cells.

**Supplemental Table S1.** List of primers used in this study.

**Supplemental Dataset S1.** IRT1 interactome determined by co-immunopurification of IRT1-mCitrine combined with mass spectrometry analyses.

798

799 **ACKNOWLEDGMENTS**

800 We thank Marc Boutry for the anti-PMA2 antibody, Mary Lou Guerinot for providing the  
801 *frd1-1* mutant, François Chaumont for the split-ubiquitin vectors, and Alexandre Martinière  
802 and Alexander Johnson for their help in image analysis. We also thank Sébastien Thomine for  
803 interesting scientific discussions. This work has benefited from the facilities and expertise of  
804 the I2BC proteomic platform SICaPS, supported by IBiSA, Ile de France Region, Plan  
805 Cancer, CNRS and Paris-Sud University and the expertise of David Cornu. The present study  
806 has also benefited from Imagerie-Gif core facility supported by Agence Nationale de la  
807 Recherche (ANR-11-EQPX-0029/Morphoscope, ANR-10-INBS-04/FranceBioImaging;  
808 ANR-11-IDEX-0003-02/ Saclay Plant Sciences).

809 **Tables**

810 **Table 1.** IRT1 interactants involved in intracellular trafficking or metal homeostasis.

811 Among the 142 putative IRT1 interacting-proteins identified by co-IP combined with mass  
812 spectrometry, we present in this table proteins that are associated to intracellular trafficking or  
813 metal homeostasis according to Gene Ontogeny (GO) annotations from The Arabidopsis  
814 Information resource (TAIR) (<https://www.arabidopsis.org>). The maximum number of unique  
815 peptides identified for each protein from the two independent experiments (see Supplemental  
816 Dataset S1) is indicated.

	Accession	Protein name	Maximum number of unique peptides
Intracellular trafficking	AT3G11130	Clathrin heavy chain	24
	AT1G04820	Tubulin alpha-4 chain	6
	AT1G29310	SecY protein transport family protein	2
	AT5G09810	Actin 7	4
	AT4G33650	Dynamin-related protein 3A	2
	AT3G63460	SEC31b, COPII component	6
	AT4G18800	RAB GTPase homolog A1D	3
	AT1G62020	Coatomer alpha subunit, COPI component	2
	AT4G31480	Coatomer beta subunit, COPI component	2
	AT4G17530	RAB GTPase homolog 1C	2
	AT1G49240	Actin 8	2
	AT5G05010	Clathrin adaptor complexes medium subunit family protein	2
	AT2G21390	Coatomer, alpha subunit, COPI component	2
	AT5G44340	Tubulin beta chain 4	2
	AT2G30050	SEC13a, COPII component	2
M	AT4G30190	H(+)-ATPase 2	13

AT4G31940	Cytochrome P450 / CYP82C4	3
AT3G13610	Feruloyl-Coenzyme A 6'-Hydroxylase 1 (F6'H1)	2
AT4G27860	Vacuolar iron transporter (VIT) family protein	11
AT5G24290	Vacuolar iron transporter (VIT) family protein	8
AT2G01530	MLP-like protein 329	5
AT1G59870	Pleiotropic drug resistance 8 / Penetration 3	4
AT1G01580	Ferric Reduction Oxidase 2	3
AT1G07890	Ascorbate peroxidase 1	2

817

818

## 819 Figure Legends

### 820 Figure 1. FRO2 and AHA2 are part of an IRT1-protein complex.

821 (A) Endogenous AHA2 is co-immunopurified with IRT1-mCitrine in *Arabidopsis* root cells.  
822 Immunopurifications (IP) were performed using anti-GFP antibodies on solubilized root  
823 protein extracts from *irt1-1/IRT1::IRT1-mCitrine* and wild-type plants (negative control).  
824 Inputs and IP fractions were subjected to immunoblotting (IB) with anti-GFP (top) and anti-  
825 AHA/PMA2 antibodies (bottom).

826 (B) mCherry-FRO2 is co-immunopurified with IRT1-mCitrine in *Arabidopsis* root cells. IP  
827 were performed using anti-GFP antibodies on solubilized root protein extracts from *irt1-1/IRT1::IRT1-mCitrine* plants co-expressing FRO2::mCherry-FRO2 or UBQ10::RabD1-mCherry, this protein co-localizing with IRT1 in endosomes (negative control). Inputs and IP  
828 fractions were subjected to IB with anti-GFP (top) and anti- mCherry antibodies (bottom).  
829 Note that mCherry-FRO2 migrates at the expected size (top band) but also at a lower  
830 molecular weight (bottom band). For the co-IP experiments in (A) and (B), roots were  
831 harvested from plants grown for 11 days on MS/2 medium containing 50  $\mu$ M Fe-EDTA, and  
832 then transferred for 4 days on MS/2 medium lacking iron and supplemented with 300  $\mu$ M of  
833 the iron chelator Ferrozine, in the presence of physiologically relevant concentrations of non-  
834 iron metal substrates. Representative immunoblots are shown.

837 (C) IRT1 directly interacts with FRO2 and AHA2 in a split-ubiquitin assay. Yeasts co-  
838 expressing Cub-PLV fusion proteins with NubG fusion proteins or NubG (negative control of  
839 interaction) or NubWT (positive control of interaction) were dropped in serial dilutions on a  
840 synthetic medium without Leu and Trp (control medium) or without Leu, Trp, His, Ade  
841 (selective medium). For the interaction tests between IRT1, FRO2, and AHA2, yeast growth  
842 on control and selective media was recorded after 24h and 48h, respectively. Besides internal

negative interaction tests performed by co-expressing Cub fusion proteins with NubG, an additional negative control was introduced in this assay by co-expressing NubG-IRT1 and BRI1-Cub. For this IRT1-BRI1 interaction test, yeast growth on control and selective media was recorded after 48h and 72h, respectively. OD: optical density. A representative assay is shown.

**Figure 2. FRO2 and AHA2 are ubiquitinated in *Arabidopsis* root cells in a metal-independent manner.**

Immunopurifications (IP) were performed using anti-GFP antibodies on solubilized root protein extracts from wild-type, *irt1-1*/IRT1::IRT1-mCitrine and Col0/35S::AHA2-GFP plants (A) or using anti-mCherry antibodies on solubilized root protein extracts from wild-type and *frd1*/FRO2::mCherry-FRO2 plants (B). Inputs and IP fractions were subjected to immunoblotting (IB) with anti-Ub antibody (P4D1) (A and B, top), anti-GFP (A, bottom), or anti-mCherry antibodies (B, bottom). Non-ubiquitinated and ubiquitinated forms of the studied proteins are indicated by an arrow and a bar (-Ub<sub>n</sub>), respectively. Roots were harvested from plants grown for 11 days on MS/2 medium lacking iron (-), in the presence of physiologically relevant concentrations of non-iron metal substrates (+), and then transferred for 2 hours to the same medium (control) or to a medium lacking iron and containing an excess of non-iron metals (+++). Wild-type plants were used as negative controls for IP. In (A), due to very low expression level, AHA2-GFP is not detected in inputs but solely in IP fractions after enrichment.

(C) Quantification of IRT1-mCitrine, AHA2-GFP, and mCherry-FRO2 ubiquitination in the presence of physiologically relevant concentrations of non-iron metal substrates (+) or an excess of these metals (+++). The intensity of the ubiquitin signal from IRT1-mCitrine, AHA2-GFP, and mCherry-FRO2 IP shown in (A) and (B) was measured using Image Lab and normalized to the quantity of immunopurified proteins. Results are shown as ratio relative to the (+) condition for each protein to reveal the influence of metal treatment.

**Figure 3. The endocytosis of IRT1 and FRO2/AHA2 is differentially regulated by non-iron metal substrates in root tip epidermal cells.**

Confocal microscopy analyses of root epidermal cells from *irt1-1/IRT1::IRT1-mCitrine* plants co-expressing IRT1::mCherry-FRO2 (**A, left panel**) or IRT1::AHA2-mCherry (**B, left panel**). Plants were grown for 11 days on MS/2 medium lacking iron, in the presence of physiologically relevant concentrations of non-iron metal substrates, and then transferred for 2 hours to the same medium (-Fe +Metals, control) or to a medium lacking iron and containing an excess of non-iron metals (-Fe +++Metals). To standardize microscopy analysis at the root tip, the same cells located just above the lateral root cap were systematically analyzed. Scale bars, 10  $\mu$ m. Representative images are shown. Right panels in (**A**) and (**B**) show the ratio of plasma membrane to intracellular signal intensities for IRT1-mCitrine, mCherry-FRO2, and AHA2-mCherry from experiments performed as in the left panels of (**A**) and (**B**).

Mander's coefficients (M2) of mCherry-FRO2 (**C**) and AHA2-mCherry (**D**) endosomal structures showing overlap with IRT1-mCitrine labeled endosomes were calculated from experiments performed as in (**A**) and (**B**), left panels. All the quantifications shown in this figure were carried out in triplicates on stacks encompassing epidermal cells. In total, 27 cells were analyzed for each condition and genotype. Error bars represent SD (n = 27) for each genotype. The asterisks indicate significant differences to -Fe +Metals (unpaired t-test, p < 0.0001).

**Figure 4. Phosphorylation of IRT1 decreases its interaction with AHA2 and FRO2. Tentative model for the functioning of the iron-acquisition complex.**

**(A-D)** Effect of IRT1 phospho-status on its interaction with AHA2 and FRO2. Split-ubiquitin interaction tests were performed between wild-type IRT1, IRT1 variants for phosphorylation sites (phosphomimic S/TxD and non-phosphorylatable S/TxA) and AHA2 (**A**), or FRO2 (**B**). Yeasts were dropped in serial dilutions on a synthetic medium without Leu and Trp (control medium) or without Leu, Trp, His, Ade (selective medium). NubG and NubWT were used as negative and positive controls of interaction, respectively. Yeast growth on control and selective medium was monitored after 48h and 72h, respectively. O.D: optical density. Representative assays are shown. To quantify interactions, the same tests were performed in liquid cultures as shown in (**C**) and (**D**). The O.D measured for transformed yeast grown in the selective medium for 24h was normalized to the O.D measured for the same yeast grown

in the control medium for 16h (relative growth). Error bars represent SEM, n = 8 in (C) and n = 12 in (D).

(E) Putative functioning of the iron-acquisition complex. IRT1, FRO2, and AHA2 proteins interact at the outer polar plasma membrane (PM) domain of root epidermal cells to form a specialized complex that likely optimizes iron acquisition by creating a local environment with low pH and high  $\text{Fe}^{2+}$  concentration. Outside this optimal zone for iron acquisition, we propose that  $\text{Fe}^{2+}$  is constantly re-oxidized to  $\text{Fe}^{3+}$ , which in turn forms insoluble iron complexes. In addition to be plasma membrane localized, the iron-acquisition complex is also probably present in early endosomes, reflecting endocytic events of the complex. Note that contrary to IRT1 and FRO2, AHA2 is distributed at both plasma membrane polar domains. FRO2 might be not exclusively associated with IRT1. This model depicts the localization of IRT1, FRO2, and AHA2 in the absence of iron and in the presence of physiologically relevant concentrations of non-iron metal substrates (–Fe +Metals). Although IRT1, FRO2, and AHA2 interact all together, this feature is not represented to simplify the scheme.

## LITERATURE CITED

- Barberon M, Dubeaux G, Kolb C, Isono E, Zelazny E, Vert G (2014) Polarization of IRON-REGULATED TRANSPORTER 1 (IRT1) to the plant-soil interface plays crucial role in metal homeostasis. *Proc Natl Acad Sci U S A* **111**: 8293-8298
- Barberon M, Zelazny E, Robert S, Conejero G, Curie C, Friml J, Vert G (2011) Monoubiquitin-dependent endocytosis of the iron-regulated transporter 1 (IRT1) transporter controls iron uptake in plants. *Proc Natl Acad Sci U S A* **108**: E450-458
- Bellati J, Champeyroux C, Hem S, Rofidal V, Krouk G, Maurel C, Santoni V (2016) Novel Aquaporin Regulatory Mechanisms Revealed by Interactomics. *Mol Cell Proteomics* **15**: 3473-3487
- Blanchet S, Cornu D, Argentini M, Namy O (2014) New insights into the incorporation of natural suppressor tRNAs at stop codons in *Saccharomyces cerevisiae*. *Nucleic Acids Res* **42**: 10061-10072
- Briat JF, Dubos C, Gaymard F (2015) Iron nutrition, biomass production, and plant product quality. *Trends Plant Sci* **20**: 33-40
- Chung KP, Zeng Y, Jiang L (2016) COPII Paralogs in Plants: Functional Redundancy or Diversity? *Trends Plant Sci* **21**: 758-769
- Cointry V, Vert G (2019) The bifunctional transporter-receptor IRT1 at the heart of metal sensing and signalling. *New Phytol* **223**: 1173-1178
- Colangelo EP, Guerinot ML (2004) The essential basic helix-loop-helix protein FIT1 is required for the iron deficiency response. *Plant Cell* **16**: 3400-3412
- Connolly EL, Campbell NH, Grotz N, Prichard CL, Guerinot ML (2003) Overexpression of the FRO2 ferric chelate reductase confers tolerance to growth on low iron and uncovers posttranscriptional control. *Plant Physiol* **133**: 1102-1110
- Couto D, Niebergall R, Liang X, Bucherl CA, Sklenar J, Macho AP, Ntoukakis V, Derbyshire P, Altenbach D, Maclean D, Robatzek S, Uhrig J, Menke F, Zhou JM, Zipfel C (2016) The

- Arabidopsis Protein Phosphatase PP2C38 Negatively Regulates the Central Immune Kinase BIK1. *PLoS Pathog* **12**: e1005811
- Dettmer J, Hong-Hermesdorf A, Stierhof YD, Schumacher K** (2006) Vacuolar H<sup>+</sup>-ATPase activity is required for endocytic and secretory trafficking in Arabidopsis. *Plant Cell* **18**: 715-730
- Dubeaux G, Neveu J, Zelazny E, Vert G** (2018) Metal Sensing by the IRT1 Transporter-Receptor Orchestrates Its Own Degradation and Plant Metal Nutrition. *Mol Cell* **69**: 953-964 e955
- Eide D, Broderius M, Fett J, Guerinot ML** (1996) A novel iron-regulated metal transporter from plants identified by functional expression in yeast. *Proceedings of the National Academy of Sciences of the United States of America* **93**: 5624-5628
- Fan L, Li R, Pan J, Ding Z, Lin J** (2015) Endocytosis and its regulation in plants. *Trends Plant Sci* **20**: 388-397
- Fourcroy P, Siso-Terraza P, Sudre D, Saviron M, Rey G, Gaymard F, Abadia A, Abadia J, Alvarez-Fernandez A, Briat JF** (2014) Involvement of the ABCG37 transporter in secretion of scopoletin and derivatives by Arabidopsis roots in response to iron deficiency. *New Phytol* **201**: 155-167
- Fourcroy P, Tissot N, Gaymard F, Briat JF, Dubos C** (2016) Facilitated Fe Nutrition by Phenolic Compounds Excreted by the Arabidopsis ABCG37/PDR9 Transporter Requires the IRT1/FRO2 High-Affinity Root Fe(2+) Transport System. *Mol Plant* **9**: 485-488
- Gao C, Luo M, Zhao Q, Yang R, Cui Y, Zeng Y, Xia J, Jiang L** (2014) A unique plant ESCRT component, FREE1, regulates multivesicular body protein sorting and plant growth. *Curr Biol* **24**: 2556-2563
- Geldner N, Denervaud-Tendon V, Hyman DL, Mayer U, Stierhof YD, Chory J** (2009) Rapid, combinatorial analysis of membrane compartments in intact plants with a multicolor marker set. *Plant J* **59**: 169-178
- Hachez C, Laloux T, Reinhardt H, Cavez D, Degand H, Grefen C, De Rycke R, Inze D, Blatt MR, Russinova E, Chaumont F** (2014) Arabidopsis SNAREs SYP61 and SYP121 coordinate the trafficking of plasma membrane aquaporin PIP2;7 to modulate the cell membrane water permeability. *Plant Cell* **26**: 3132-3147
- Haruta M, Tan LX, Bushey DB, Swanson SJ, Sussman MR** (2018) Environmental and Genetic Factors Regulating Localization of the Plant Plasma Membrane H<sup>(+)</sup>-ATPase. *Plant Physiol* **176**: 364-377
- Hoffmann RD, Olsen LI, Ezike CV, Pedersen JT, Manstretta R, Lopez-Marques RL, Palmgren M** (2018) Roles of plasma membrane proton ATPases AHA2 and AHA7 in normal growth of roots and root hairs in Arabidopsis thaliana. *Physiol Plant*
- Inoue H, Kobayashi T, Nozoye T, Takahashi M, Kakei Y, Suzuki K, Nakazono M, Nakanishi H, Mori S, Nishizawa NK** (2009) Rice OsYSL15 is an iron-regulated iron(III)-deoxymugineic acid transporter expressed in the roots and is essential for iron uptake in early growth of the seedlings. *J Biol Chem* **284**: 3470-3479
- Ishimaru Y, Kim S, Tsukamoto T, Oki H, Kobayashi T, Watanabe S, Matsuhashi S, Takahashi M, Nakanishi H, Mori S, Nishizawa NK** (2007) Mutational reconstructed ferric chelate reductase confers enhanced tolerance in rice to iron deficiency in calcareous soil. *Proc Natl Acad Sci U S A* **104**: 7373-7378
- Ishimaru Y, Suzuki M, Tsukamoto T, Suzuki K, Nakazono M, Kobayashi T, Wada Y, Watanabe S, Matsuhashi S, Takahashi M, Nakanishi H, Mori S, Nishizawa NK** (2006) Rice plants take up iron as an Fe<sup>3+</sup>-phytosiderophore and as Fe<sup>2+</sup>. *Plant J* **45**: 335-346
- Ivanov R, Brumbarova T, Blum A, Jantke AM, Fink-Straube C, Bauer P** (2014) SORTING NEXIN1 Is Required for Modulating the Trafficking and Stability of the Arabidopsis IRON-REGULATED TRANSPORTER1. *Plant Cell* **26**: 1294-1307
- Jakoby M, Wang HY, Reidt W, Weisshaar B, Bauer P** (2004) FRU (BHLH029) is required for induction of iron mobilization genes in Arabidopsis thaliana. *FEBS Lett* **577**: 528-534
- Jeong J, Merkovich A, Clyne M, Connolly EL** (2017) Directing iron transport in dicots: regulation of iron acquisition and translocation. *Curr Opin Plant Biol* **39**: 106-113



997 **Johnson A, Vert G** (2016) Unraveling K63 Polyubiquitination Networks by Sensor-Based Proteomics.  
 998 *Plant Physiol* **171**: 1808-1820

999 **Karlova R, Boeren S, Russinova E, Aker J, Vervoort J, de Vries S** (2006) The Arabidopsis SOMATIC  
 1000 EMBRYOGENESIS RECEPTOR-LIKE KINASE1 protein complex includes BRASSINOSTEROID-  
 1001 INSENSITIVE1. *Plant Cell* **18**: 626-638

1002 **Khan I, Gratz R, Denezhkin P, Schott-Verdugo SN, Angrand K, Genders L, Basgaran RM, Fink-Straube  
 1003 C, Brumbarova T, Gohlke H, Bauer P, Ivanov R** (2019) Calcium-promoted interaction  
 1004 between the C2-domain protein EHB1 and metal transporter IRT1 inhibits Arabidopsis iron  
 1005 acquisition. *Plant Physiol*

1006 **Kim DY, Bovet L, Maeshima M, Martinoia E, Lee Y** (2007) The ABC transporter AtPDR8 is a cadmium  
 1007 extrusion pump conferring heavy metal resistance. *Plant J* **50**: 207-218

1008 **Kim DY, Scalf M, Smith LM, Vierstra RD** (2013) Advanced proteomic analyses yield a deep catalog of  
 1009 ubiquitylation targets in Arabidopsis. *Plant Cell* **25**: 1523-1540

1010 **Komander D** (2009) The emerging complexity of protein ubiquitination. *Biochem Soc Trans* **37**: 937-  
 1011 953

1012 **Kwok EY, Severance S, Kosman DJ** (2006) Evidence for iron channeling in the Fet3p-Ftr1p high-  
 1013 affinity iron uptake complex in the yeast plasma membrane. *Biochemistry* **45**: 6317-6327

1014 **Lauwers E, Erpapazoglou Z, Haguenaer-Tsapis R, Andre B** (2010) The ubiquitin code of yeast  
 1015 permease trafficking. *Trends Cell Biol* **20**: 196-204

1016 **Lee S, Chiecko JC, Kim SA, Walker EL, Lee Y, Guerinot ML, An G** (2009) Disruption of OsYSL15 leads  
 1017 to iron inefficiency in rice plants. *Plant Physiol* **150**: 786-800

1018 **Marques-Bueno MDM, Morao AK, Cayrel A, Platre MP, Barberon M, Caillieux E, Colot V, Jaillais Y,  
 1019 Roudier F, Vert G** (2016) A versatile Multisite Gateway-compatible promoter and transgenic  
 1020 line collection for cell type-specific functional genomics in Arabidopsis. *Plant J* **85**: 320-333

1021 **Martins S, Dohmann EM, Cayrel A, Johnson A, Fischer W, Pojer F, Satiat-Jeunemaitre B, Jaillais Y,  
 1022 Chory J, Geldner N, Vert G** (2015) Internalization and vacuolar targeting of the  
 1023 brassinosteroid hormone receptor BRI1 are regulated by ubiquitination. *Nat Commun* **6**:  
 1024 6151

1025 **Masalkar P, Wallace IS, Hwang JH, Roberts DM** (2010) Interaction of cytosolic glutamine synthetase  
 1026 of soybean root nodules with the C-terminal domain of the symbiosome membrane nodulin  
 1027 26 aquaglyceroporin. *J Biol Chem* **285**: 23880-23888

1028 **Morsomme P, Dambly S, Maudoux O, Boutry M** (1998) Single point mutations distributed in 10  
 1029 soluble and membrane regions of the *Nicotiana plumbaginifolia* plasma membrane PMA2  
 1030 H<sup>+</sup>-ATPase activate the enzyme and modify the structure of the C-terminal region. *J Biol*  
 1031 *Chem* **273**: 34837-34842

1032 **Olsen RA, Clark RB, Bennett JH** (1981) THE ENHANCEMENT OF SOIL FERTILITY BY PLANT-ROOTS.  
 1033 *American Scientist* **69**: 378-384

1034 **Pacifici E, Di Mambro R, Dello Iorio R, Costantino P, Sabatini S** (2018) Acidic cell elongation drives cell  
 1035 differentiation in the Arabidopsis root. *EMBO J* **37**

1036 **Palmer CM, Guerinot ML** (2009) Facing the challenges of Cu, Fe and Zn homeostasis in plants. *Nat*  
 1037 *Chem Biol* **5**: 333-340

1038 **Qi X, Zheng H** (2013) Rab-A1c GTPase defines a population of the trans-Golgi network that is  
 1039 sensitive to endosidin1 during cytokinesis in Arabidopsis. *Mol Plant* **6**: 847-859

1040 **Rajniak J, Giehl RFH, Chang E, Murgia I, von Wiren N, Sattely ES** (2018) Biosynthesis of redox-active  
 1041 metabolites in response to iron deficiency in plants. *Nat Chem Biol* **14**: 442-450

1042 **Robinson NJ, Procter CM, Connolly EL, Guerinot ML** (1999) A ferric-chelate reductase for iron uptake  
 1043 from soils. *Nature* **397**: 694-697

1044 **Rodriguez-Celma J, Lin WD, Fu GM, Abadia J, Lopez-Millan AF, Schmidt W** (2013) Mutually exclusive  
 1045 alterations in secondary metabolism are critical for the uptake of insoluble iron compounds  
 1046 by Arabidopsis and *Medicago truncatula*. *Plant Physiol* **162**: 1473-1485

1047 **Rogers EE, Eide DJ, Guerinot ML** (2000) Altered selectivity in an Arabidopsis metal transporter. *Proc*  
 1048 *Natl Acad Sci U S A* **97**: 12356-12360

1049 **Santi S, Schmidt W** (2009) Dissecting iron deficiency-induced proton extrusion in Arabidopsis roots.  
 1050 *New Phytol* **183**: 1072-1084

1051 **Schmid NB, Giehl RF, Doll S, Mock HP, Strehmel N, Scheel D, Kong X, Hider RC, von Wiren N** (2014)  
 1052 Feruloyl-CoA 6'-Hydroxylase1-dependent coumarins mediate iron acquisition from alkaline  
 1053 substrates in Arabidopsis. *Plant Physiol* **164**: 160-172

1054 **Shin LJ, Lo JC, Chen GH, Callis J, Fu H, Yeh KC** (2013) IRT1 degradation factor1, a ring E3 ubiquitin  
 1055 ligase, regulates the degradation of iron-regulated transporter1 in Arabidopsis. *Plant Cell* **25**:  
 1056 3039-3051

1057 **Singh A, Severance S, Kaur N, Wiltsie W, Kosman DJ** (2006) Assembly, activation, and trafficking of  
 1058 the Fet3p.Ftr1p high affinity iron permease complex in *Saccharomyces cerevisiae*. *J Biol*  
 1059 *Chem* **281**: 13355-13364

1060 **Tan S, Zhang P, Xiao W, Feng B, Chen LY, Li S, Li P, Zhao WZ, Qi XT, Yin LP** (2018) TMD1 domain and  
 1061 CRAC motif determine the association and disassociation of MxIRT1 with detergent-resistant  
 1062 membranes. *Traffic* **19**: 122-137

1063 **Thomine S, Vert G** (2013) Iron transport in plants: better be safe than sorry. *Curr Opin Plant Biol* **16**:  
 1064 322-327

1065 **Vert G, Briat JF, Curie C** (2001) Arabidopsis IRT2 gene encodes a root-periphery iron transporter.  
 1066 *Plant Journal* **26**: 181-189

1067 **Vert G, Grotz N, Dedaldechamp F, Gaymard F, Guerinot ML, Briat JF, Curie C** (2002) IRT1, an  
 1068 Arabidopsis transporter essential for iron uptake from the soil and for plant growth. *Plant*  
 1069 *Cell* **14**: 1223-1233

1070 **von der Haar T** (2007) Optimized protein extraction for quantitative proteomics of yeasts. *PLoS One*  
 1071 **2**: e1078

1072 **Walton A, Stes E, Cybulski N, Van Bel M, Inigo S, Durand AN, Timmerman E, Heyman J, Pauwels L,**  
 1073 **De Veylder L, Goossens A, De Smet I, Coppens F, Goormachtig S, Gevaert K** (2016) It's Time  
 1074 for Some "Site"-Seeing: Novel Tools to Monitor the Ubiquitin Landscape in Arabidopsis  
 1075 thaliana. *Plant Cell* **28**: 6-16

1076 **Xing S, Wallmeroth N, Berendzen KW, Grefen C** (2016) Techniques for the Analysis of Protein-  
 1077 Protein Interactions in Vivo. *Plant Physiol* **171**: 727-758

1078 **Yamada K, Nagano AJ, Nishina M, Hara-Nishimura I, Nishimura M** (2013) Identification of two novel  
 1079 endoplasmic reticulum body-specific integral membrane proteins. *Plant Physiol* **161**: 108-120

1080 **Yi Y, Guerinot ML** (1996) Genetic evidence that induction of root Fe(III) chelate reductase activity is  
 1081 necessary for iron uptake under iron deficiency. *Plant J.* **10**: 835-844

1082 **Yorimitsu T, Sato K, Takeuchi M** (2014) Molecular mechanisms of Sar/Arf GTPases in vesicular  
 1083 trafficking in yeast and plants. *Front Plant Sci* **5**: 411

1084 **Yuan W, Zhang D, Song T, Xu F, Lin S, Xu W, Li Q, Zhu Y, Liang J, Zhang J** (2017) Arabidopsis plasma  
 1085 membrane H<sup>+</sup>-ATPase genes AHA2 and AHA7 have distinct and overlapping roles in the  
 1086 modulation of root tip H<sup>+</sup> efflux in response to low-phosphorus stress. *J Exp Bot* **68**: 1731-  
 1087 1741

1088 **Yuan Y, Wu H, Wang N, Li J, Zhao W, Du J, Wang D, Ling HQ** (2008) FIT interacts with AtbHLH38 and  
 1089 AtbHLH39 in regulating iron uptake gene expression for iron homeostasis in Arabidopsis. *Cell*  
 1090 *Res* **18**: 385-397

1091 **Zelazny E, Barberon M, Curie C, Vert G** (2011) Ubiquitination of transporters at the forefront of plant  
 1092 nutrition. *Plant Signal Behav* **6**: 1597-1599

1093 **Zelazny E, Borst JW, Muylaert M, Batoko H, Hemminga MA, Chaumont F** (2007) FRET imaging in  
 1094 living maize cells reveals that plasma membrane aquaporins interact to regulate their  
 1095 subcellular localization. *Proc Natl Acad Sci U S A* **104**: 12359-12364

1096 **Zelazny E, Micielica U, Borst JW, Hemminga MA, Chaumont F** (2009) An N-terminal diacidic motif is  
 1097 required for the trafficking of maize aquaporins ZmPIP2;4 and ZmPIP2;5 to the plasma  
 1098 membrane. *Plant J* **57**: 346-355

1099 **Zhang J, Li W, Xiang T, Liu Z, Laluk K, Ding X, Zou Y, Gao M, Zhang X, Chen S, Mengiste T, Zhang Y,**  
 1100 **Zhou JM** (2010) Receptor-like cytoplasmic kinases integrate signaling from multiple plant

1101 immune receptors and are targeted by a *Pseudomonas syringae* effector. *Cell Host Microbe*  
1102 **7**: 290-301  
1103

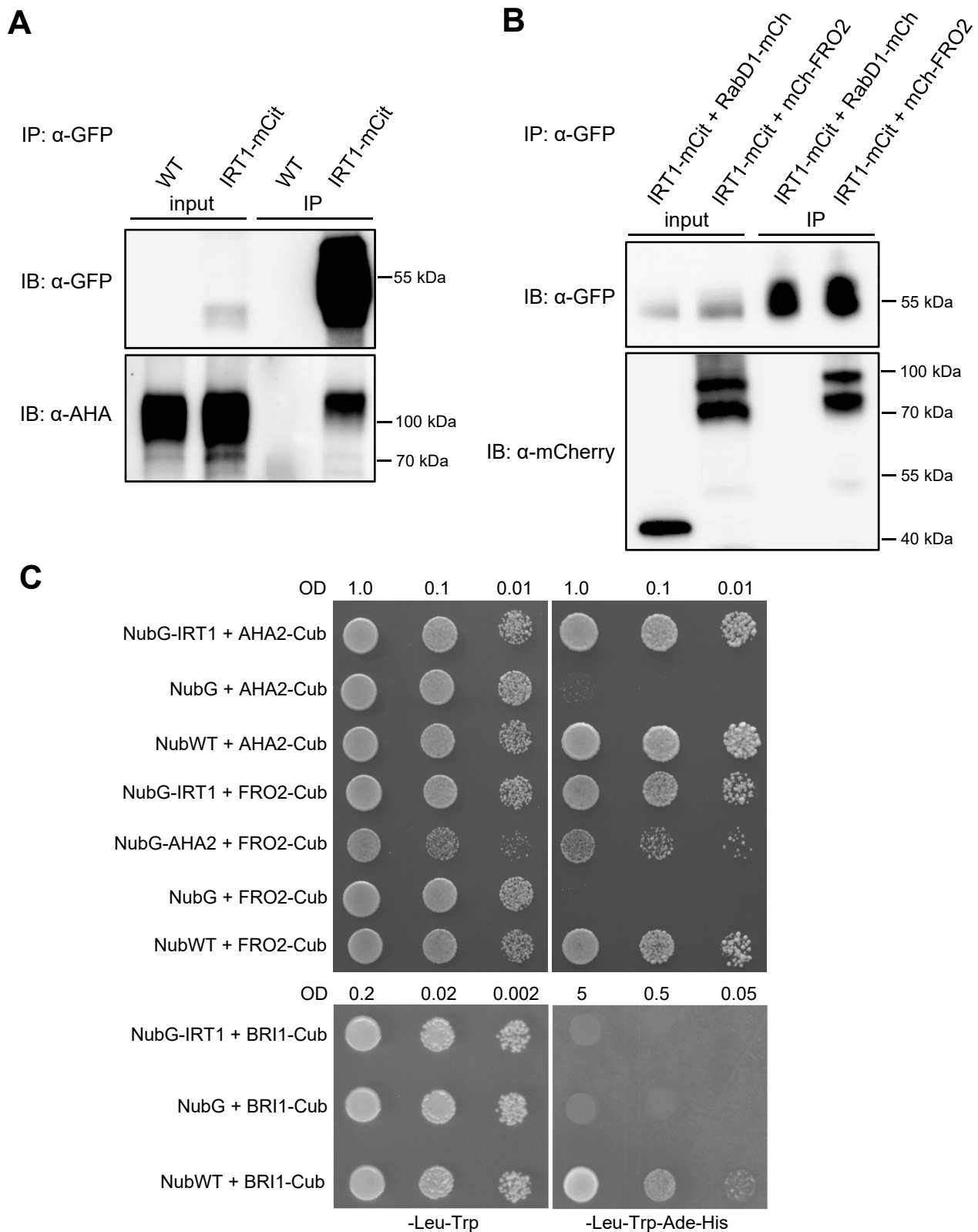


**Figure 1. FRO2 and AHA2 are part of an IRT1-protein complex.**

(A) Endogenous AHA2 is co-immunopurified with IRT1-mCitrine in *Arabidopsis* root cells. Immunopurifications (IP) were performed using anti-GFP antibodies on solubilized root protein extracts from *irt1-1*/IRT1::IRT1-mCitrine and wild-type plants (negative control). Inputs and IP fractions were subjected to immunoblotting (IB) with anti-GFP (top) and anti-AHA/PMA2 antibodies (bottom).

**Figure 1. (continued)**

**(B)** mCherry-FRO2 is co-immunopurified with IRT1-mCitrine in *Arabidopsis* root cells. IP were performed using anti-GFP antibodies on solubilized root protein extracts from *irt1-1*/IRT1::IRT1-mCitrine plants co-expressing FRO2::mCherry-FRO2 or UBQ10::RabD1-mCherry, this protein co-localizing with IRT1 in endosomes (negative control). Inputs and IP fractions were subjected to IB with anti-GFP (top) and anti-mCherry antibodies (bottom). Note that mCherry-FRO2 migrates at the expected size (top band) but also at a lower molecular weight (bottom band). For the co-IP experiments in (A) and (B), roots were harvested from plants grown for 11 days on MS/2 medium containing 50  $\mu$ M Fe-EDTA, and then transferred for 4 days on MS/2 medium lacking iron and supplemented with 300  $\mu$ M of the iron chelator Ferrozine, in the presence of physiologically relevant concentrations of non-iron metal substrates. Representative immunoblots are shown.

**(C)** IRT1 directly interacts with FRO2 and AHA2 in a split-ubiquitin assay. Yeasts co-expressing Cub-PLV fusion proteins with NubG fusion proteins or NubG (negative control of interaction) or NubWT (positive control of interaction) were dropped in serial dilutions on a synthetic medium without Leu and Trp (control medium) or without Leu, Trp, His, Ade (selective medium). For the interaction tests between IRT1, FRO2, and AHA2, yeast growth on control and selective media was recorded after 24h and 48h, respectively. Besides internal negative interaction tests performed by co-expressing Cub fusion proteins with NubG, an additional negative control was introduced in this assay by co-expressing NubG-IRT1 and BRI1-Cub. For this IRT1-BRI1 interaction test, yeast growth on control and selective media was recorded after 48h and 72h, respectively. OD: optical density. A representative assay is shown.

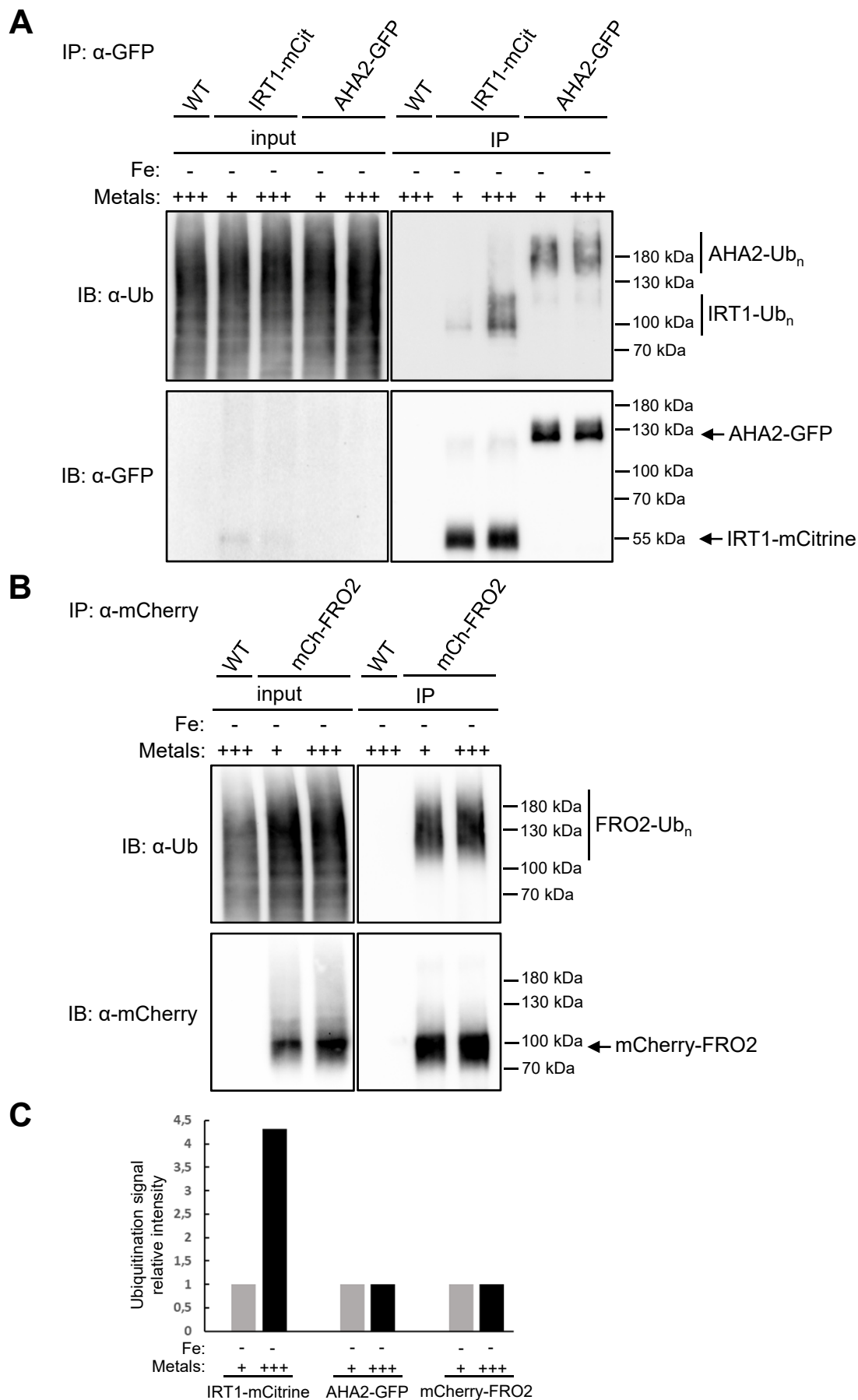


**Figure 2. FRO2 and AHA2 are ubiquitinated in *Arabidopsis* root cells in a metal-independent manner.**

Immunopurifications (IP) were performed using anti-GFP antibodies on solubilized root protein extracts from wild-type, *irt1-1*/IRT1::IRT1-mCitrine and Col0/35S::AHA2-GFP plants (A) or using anti-mCherry antibodies on solubilized root protein extracts from wild-type and *frd1*/FRO2::mCherry-FRO2 plants (B).

**Figure 2 (continued).**

Inputs and IP fractions were subjected to immunoblotting (IB) with anti-Ub antibody (P4D1) (A and B, top), anti-GFP (A, bottom), or anti-mCherry antibodies (B, bottom). Non-ubiquitinated and ubiquitinated forms of the studied proteins are indicated by an arrow and a bar (-Ub<sub>n</sub>), respectively. Roots were harvested from plants grown for 11 days on MS/2 medium lacking iron (-), in the presence of physiologically relevant concentrations of non-iron metal substrates (+), and then transferred for 2 hours to the same medium (control) or to a medium lacking iron and containing an excess of non-iron metals (+++). Wild-type plants were used as negative controls for IP. In (A), due to very low expression level, AHA2-GFP is not detected in inputs but solely in IP fractions after enrichment. (C) Quantification of IRT1-mCitrine, AHA2-GFP, and mCherry-FRO2 ubiquitination in the presence of physiologically relevant concentrations of non-iron metal substrates (+) or an excess of these metals (+++). The intensity of the ubiquitin signal from IRT1-mCitrine, AHA2-GFP, and mCherry-FRO2 IP shown in (A) and (B) was measured using Image Lab and normalized to the quantity of immunopurified proteins. Results are shown as ratio relative to the (+) condition for each protein to reveal the influence of metal treatment.

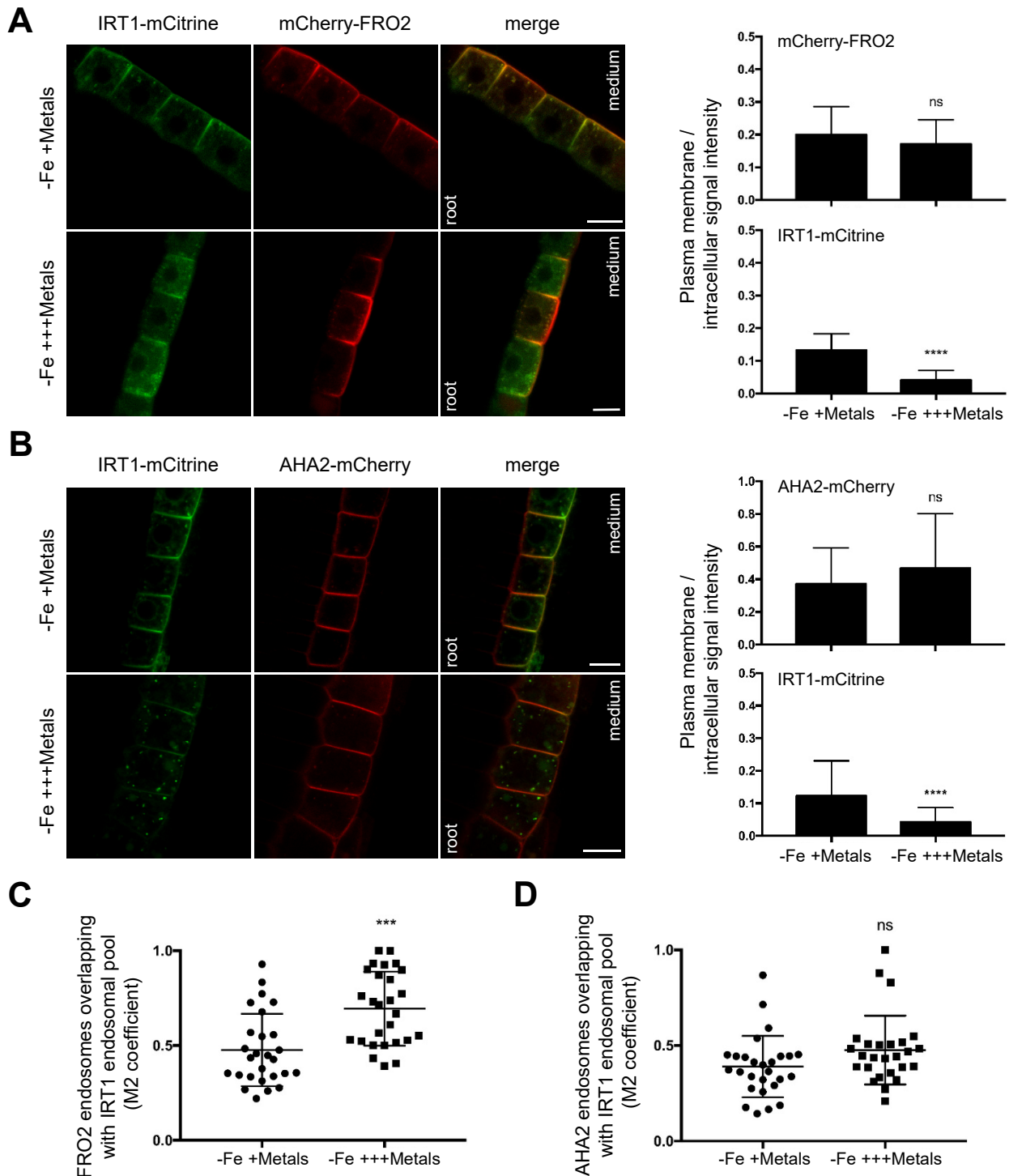


**Figure 3. The endocytosis of IRT1 and FRO2/AHA2 is differentially regulated by non-iron metal substrates in root tip epidermal cells.**

Confocal microscopy analyses of root epidermal cells from *irt1-1/IRT1::IRT1-mCitrine* plants co-expressing IRT1::mCherry-FRO2 (**A, left panel**) or IRT1::AHA2-mCherry (**B, left panel**). Plants were grown for 11 days on MS/2 medium lacking iron, in the presence of physiologically relevant concentrations of non-iron metal substrates, and then transferred for 2 hours to the same medium (-Fe +Metals, control) or to a medium lacking iron and containing an excess of non-iron metals (-Fe +++Metals). To standardize microscopy analysis at the root tip, the same cells located just above the lateral root cap were systematically analyzed. Scale bars, 10  $\mu$ m. Representative images are shown. Right panels in (**A**) and (**B**) show the ratio of plasma membrane to intracellular signal intensities for IRT1-mCitrine, mCherry-FRO2, and AHA2-mCherry from experiments performed as in the left panels of (**A**) and (**B**). Mander's coefficients (M2) of mCherry-FRO2 (**C**) and AHA2-mCherry (**D**) endosomal structures showing overlap with IRT1-mCitrine labeled endosomes were calculated from experiments performed as in (**A**) and (**B**), left panels. All the quantifications shown in this figure were carried out in triplicates on stacks encompassing epidermal cells. In total, 27 cells were analyzed for each condition and genotype. Error bars represent SD ( $n = 27$ ) for each genotype. The asterisks indicate significant differences to -Fe +Metals (unpaired t-test,  $p < 0.0001$ ).



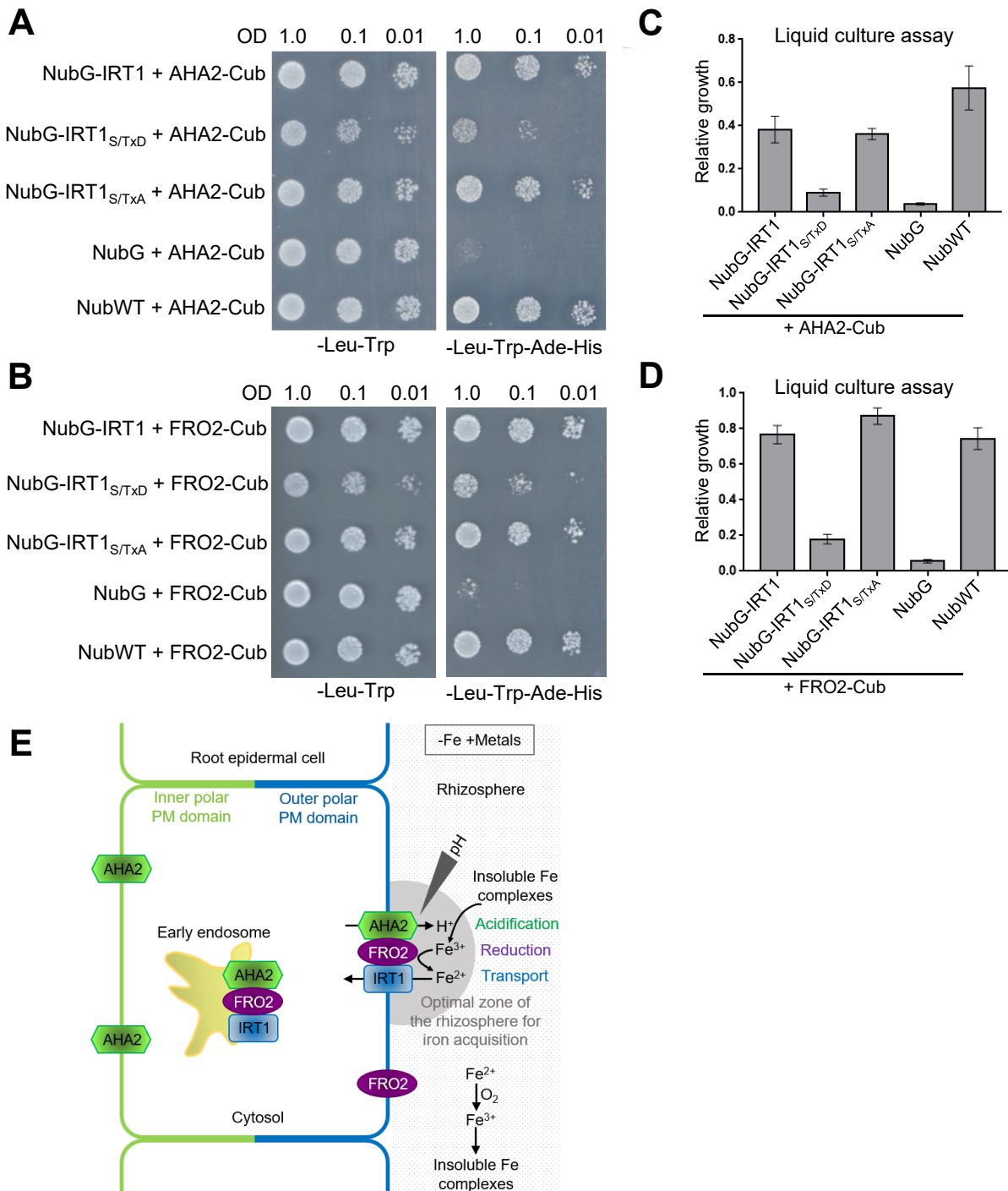


**Figure 4. Phosphorylation of IRT1 decreases its interaction with AHA2 and FRO2. Tentative model for the functioning of the iron-acquisition complex.**

(A–D) Effect of IRT1 phospho-status on its interaction with AHA2 and FRO2. Split-ubiquitin interaction tests were performed between wild-type IRT1, IRT1 variants for phosphorylation sites (phosphomimic S/TxD and non-phosphorylatable S/TxA) and AHA2 (A), or FRO2 (B). Yeasts were dropped in serial dilutions on a synthetic medium without Leu and Trp (control medium) or without Leu, Trp, His, Ade (selective medium). NubG and NubWT were used as negative and positive controls of interaction, respectively. Yeast growth on control and selective medium was monitored after 48h and 72h, respectively. O.D: optical density. Representative assays are shown. To quantify interactions, the same tests were performed in liquid cultures as shown in (C) and (D). The O.D measured for transformed yeast grown in the selective medium for 24h was normalized to the O.D measured for the same yeast grown in the control medium for 16h (relative growth). Error bars represent SEM,  $n = 8$  in (C) and  $n = 12$  in (D).

**Figure 4 (continued)**

**(E)** Putative functioning of the iron-acquisition complex. IRT1, FRO2 and AHA2 proteins interact at the outer polar plasma membrane (PM) domain of root epidermal cells to form a specialized complex that likely optimizes iron acquisition by creating a local environment with low pH and high  $\text{Fe}^{2+}$  concentration. Outside this optimal zone for iron acquisition, we propose that  $\text{Fe}^{2+}$  is constantly re-oxidized to  $\text{Fe}^{3+}$ , which in turn forms insoluble iron complexes. In addition to be plasma membrane localized, the iron-acquisition complex is also probably present in early endosomes, reflecting endocytic events of the complex. Note that contrary to IRT1 and FRO2, AHA2 is distributed at both plasma membrane polar domains. FRO2 might be not exclusively associated with IRT1. This model depicts the localization of IRT1, FRO2, and AHA2 in the absence of iron and in the presence of physiologically relevant concentrations of non-iron metal substrates (–Fe +Metals). Although IRT1, FRO2, and AHA2 interact all together, this feature is not represented to simplify the scheme.

## Parsed Citations

Barberon M, Dubeaux G, Kolb C, Isono E, Zelazny E, Vert G (2014) Polarization of IRON-REGULATED TRANSPORTER 1 (IRT1) to the plant-soil interface plays crucial role in metal homeostasis. *Proc Natl Acad Sci U S A* 111: 8293-8298

Google Scholar: [Author Only](#) [Title Only](#) [Author and Title](#)

Barberon M, Zelazny E, Robert S, Conejero G, Curie C, Friml J, Vert G (2011) Monoubiquitin-dependent endocytosis of the iron-regulated transporter 1 (IRT1) transporter controls iron uptake in plants. *Proc Natl Acad Sci U S A* 108: E450-458

Google Scholar: [Author Only](#) [Title Only](#) [Author and Title](#)

Bellati J, Champeyroux C, Hem S, Rofidal V, Krouk G, Maurel C, Santoni V (2016) Novel Aquaporin Regulatory Mechanisms Revealed by Interactomics. *Mol Cell Proteomics* 15: 3473-3487

Google Scholar: [Author Only](#) [Title Only](#) [Author and Title](#)

Blanchet S, Cornu D, Argentini M, Namy O (2014) New insights into the incorporation of natural suppressor tRNAs at stop codons in *Saccharomyces cerevisiae*. *Nucleic Acids Res* 42: 10061-10072

Google Scholar: [Author Only](#) [Title Only](#) [Author and Title](#)

Briat JF, Dubos C, Gaymard F (2015) Iron nutrition, biomass production, and plant product quality. *Trends Plant Sci* 20: 33-40

Google Scholar: [Author Only](#) [Title Only](#) [Author and Title](#)

Chung KP, Zeng Y, Jiang L (2016) COPII Paralogs in Plants: Functional Redundancy or Diversity? *Trends Plant Sci* 21: 758-769

Google Scholar: [Author Only](#) [Title Only](#) [Author and Title](#)

Cointry V, Vert G (2019) The bifunctional transporter-receptor IRT1 at the heart of metal sensing and signalling. *New Phytol* 223: 1173-1178

Google Scholar: [Author Only](#) [Title Only](#) [Author and Title](#)

Colangelo EP, Guerinot ML (2004) The essential basic helix-loop-helix protein FIT1 is required for the iron deficiency response. *Plant Cell* 16: 3400-3412

Google Scholar: [Author Only](#) [Title Only](#) [Author and Title](#)

Connolly EL, Campbell NH, Grotz N, Prichard CL, Guerinot ML (2003) Overexpression of the FRO2 ferric chelate reductase confers tolerance to growth on low iron and uncovers posttranscriptional control. *Plant Physiol* 133: 1102-1110

Google Scholar: [Author Only](#) [Title Only](#) [Author and Title](#)

Couto D, Niebergall R, Liang X, Bucherl CA, Sklenar J, Macho AP, Ntoukakis V, Derbyshire P, Altenbach D, Maclean D, Robatzek S, Uhrig J, Menke F, Zhou JM, Zipfel C (2016) The Arabidopsis Protein Phosphatase PP2C38 Negatively Regulates the Central Immune Kinase BIK1. *PLoS Pathog* 12: e1005811

Google Scholar: [Author Only](#) [Title Only](#) [Author and Title](#)

Dettmer J, Hong-Hermesdorf A, Stierhof YD, Schumacher K (2006) Vacuolar H<sup>+</sup>-ATPase activity is required for endocytic and secretory trafficking in Arabidopsis. *Plant Cell* 18: 715-730

Google Scholar: [Author Only](#) [Title Only](#) [Author and Title](#)

Dubeaux G, Neveu J, Zelazny E, Vert G (2018) Metal Sensing by the IRT1 Transporter-Receptor Orchestrates Its Own Degradation and Plant Metal Nutrition. *Mol Cell* 69: 953-964 e955

Google Scholar: [Author Only](#) [Title Only](#) [Author and Title](#)

Eide D, Broderius M, Fett J, Guerinot ML (1996) A novel iron-regulated metal transporter from plants identified by functional expression in yeast. *Proceedings of the National Academy of Sciences of the United States of America* 93: 5624-5628

Google Scholar: [Author Only](#) [Title Only](#) [Author and Title](#)

Fan L, Li R, Pan J, Ding Z, Lin J (2015) Endocytosis and its regulation in plants. *Trends Plant Sci* 20: 388-397

Google Scholar: [Author Only](#) [Title Only](#) [Author and Title](#)

Fourcroy P, Siso-Terraza P, Sudre D, Saviron M, Rey G, Gaymard F, Abadia A, Abadia J, Alvarez-Fernandez A, Briat JF (2014) Involvement of the ABCG37 transporter in secretion of scopoletin and derivatives by Arabidopsis roots in response to iron deficiency. *New Phytol* 201: 155-167

Google Scholar: [Author Only](#) [Title Only](#) [Author and Title](#)

Fourcroy P, Tissot N, Gaymard F, Briat JF, Dubos C (2016) Facilitated Fe Nutrition by Phenolic Compounds Excreted by the Arabidopsis ABCG37/PDR9 Transporter Requires the IRT1/FRO2 High-Affinity Root Fe(2+) Transport System. *Mol Plant* 9: 485-488

Google Scholar: [Author Only](#) [Title Only](#) [Author and Title](#)

Gao C, Luo M, Zhao Q, Yang R, Cui Y, Zeng Y, Xia J, Jiang L (2014) A unique plant ESCRT component, FREE1, regulates multivesicular body protein sorting and plant growth. *Curr Biol* 24: 2556-2563

Google Scholar: [Author Only](#) [Title Only](#) [Author and Title](#)

Geldner N, Denervaud-Tendon V, Hyman DL, Mayer U, Stierhof YD, Chory J (2009) Rapid, combinatorial analysis of membrane

compartments in intact plants with a multicolor marker set. *Plant J* 59: 169-178

Google Scholar: [Author Only](#) [Title Only](#) [Author and Title](#)

Hachez C, Laloux T, Reinhardt H, Cavez D, Degand H, Grefen C, De Rycke R, Inze D, Blatt MR, Russinova E, Chaumont F (2014) *Arabidopsis* SNAREs SYP61 and SYP121 coordinate the trafficking of plasma membrane aquaporin PIP2;7 to modulate the cell membrane water permeability. *Plant Cell* 26: 3132-3147

Google Scholar: [Author Only](#) [Title Only](#) [Author and Title](#)

Haruta M, Tan LX, Bushey DB, Swanson SJ, Sussman MR (2018) Environmental and Genetic Factors Regulating Localization of the Plant Plasma Membrane H(+)-ATPase. *Plant Physiol* 176: 364-377

Google Scholar: [Author Only](#) [Title Only](#) [Author and Title](#)

Hoffmann RD, Olsen LI, Ezike CV, Pedersen JT, Manstretta R, Lopez-Marques RL, Palmgren M (2018) Roles of plasma membrane proton ATPases AHA2 and AHA7 in normal growth of roots and root hairs in *Arabidopsis thaliana*. *Physiol Plant*

Google Scholar: [Author Only](#) [Title Only](#) [Author and Title](#)

Inoue H, Kobayashi T, Nozoye T, Takahashi M, Kakei Y, Suzuki K, Nakazono M, Nakanishi H, Mori S, Nishizawa NK (2009) Rice OsYSL15 is an iron-regulated iron(III)-deoxymugineic acid transporter expressed in the roots and is essential for iron uptake in early growth of the seedlings. *J Biol Chem* 284: 3470-3479

Google Scholar: [Author Only](#) [Title Only](#) [Author and Title](#)

Ishimaru Y, Kim S, Tsukamoto T, Oki H, Kobayashi T, Watanabe S, Matsushashi S, Takahashi M, Nakanishi H, Mori S, Nishizawa NK (2007) Mutational reconstructed ferric chelate reductase confers enhanced tolerance in rice to iron deficiency in calcareous soil. *Proc Natl Acad Sci U S A* 104: 7373-7378

Google Scholar: [Author Only](#) [Title Only](#) [Author and Title](#)

Ishimaru Y, Suzuki M, Tsukamoto T, Suzuki K, Nakazono M, Kobayashi T, Wada Y, Watanabe S, Matsushashi S, Takahashi M, Nakanishi H, Mori S, Nishizawa NK (2006) Rice plants take up iron as an Fe<sup>3+</sup>-phytosiderophore and as Fe<sup>2+</sup>. *Plant J* 45: 335-346

Google Scholar: [Author Only](#) [Title Only](#) [Author and Title](#)

Ivanov R, Brumbarova T, Blum A, Jantke AM, Fink-Straube C, Bauer P (2014) SORTING NEXIN1 Is Required for Modulating the Trafficking and Stability of the *Arabidopsis* IRON-REGULATED TRANSPORTER1. *Plant Cell* 26: 1294-1307

Google Scholar: [Author Only](#) [Title Only](#) [Author and Title](#)

Jakoby M, Wang HY, Reidt W, Weisshaar B, Bauer P (2004) FRU (BHLH029) is required for induction of iron mobilization genes in *Arabidopsis thaliana*. *FEBS Lett* 577: 528-534

Google Scholar: [Author Only](#) [Title Only](#) [Author and Title](#)

Jeong J, Merkovich A, Clyne M, Connolly EL (2017) Directing iron transport in dicots: regulation of iron acquisition and translocation. *Curr Opin Plant Biol* 39: 106-113

Google Scholar: [Author Only](#) [Title Only](#) [Author and Title](#)

Johnson A, Vert G (2016) Unraveling K63 Polyubiquitination Networks by Sensor-Based Proteomics. *Plant Physiol* 171: 1808-1820

Google Scholar: [Author Only](#) [Title Only](#) [Author and Title](#)

Karlova R, Boeren S, Russinova E, Aker J, Vervoort J, de Vries S (2006) The *Arabidopsis* SOMATIC EMBRYOGENESIS RECEPTOR-LIKE KINASE1 protein complex includes BRASSINOSTEROID-INSENSITIVE1. *Plant Cell* 18: 626-638

Google Scholar: [Author Only](#) [Title Only](#) [Author and Title](#)

Khan I, Gratz R, Denezhkin P, Schott-Verdugo SN, Angrand K, Genders L, Basgaran RM, Fink-Straube C, Brumbarova T, Gohlke H, Bauer P, Ivanov R (2019) Calcium-promoted interaction between the C2-domain protein EHB1 and metal transporter IRT1 inhibits *Arabidopsis* iron acquisition. *Plant Physiol*

Google Scholar: [Author Only](#) [Title Only](#) [Author and Title](#)

Kim DY, Bovet L, Maeshima M, Martinoia E, Lee Y (2007) The ABC transporter AtPDR8 is a cadmium extrusion pump conferring heavy metal resistance. *Plant J* 50: 207-218

Google Scholar: [Author Only](#) [Title Only](#) [Author and Title](#)

Kim DY, Scalf M, Smith LM, Vierstra RD (2013) Advanced proteomic analyses yield a deep catalog of ubiquitylation targets in *Arabidopsis*. *Plant Cell* 25: 1523-1540

Google Scholar: [Author Only](#) [Title Only](#) [Author and Title](#)

Komander D (2009) The emerging complexity of protein ubiquitination. *Biochem Soc Trans* 37: 937-953

Google Scholar: [Author Only](#) [Title Only](#) [Author and Title](#)

Kwok EY, Severance S, Kosman DJ (2006) Evidence for iron channeling in the Fet3p-Ftr1p high-affinity iron uptake complex in the yeast plasma membrane. *Biochemistry* 45: 6317-6327

Google Scholar: [Author Only](#) [Title Only](#) [Author and Title](#)

Lauwers E, Erpapazoglou Z, Haguenauer-Tsapis R, Andre B (2010) The ubiquitin code of yeast permease trafficking. *Trends Cell*

Google Scholar: [Author Only](#) [Title Only](#) [Author and Title](#)

Lee S, Chiecko JC, Kim SA, Walker EL, Lee Y, Guerinot ML, An G (2009) Disruption of OsYSL15 leads to iron inefficiency in rice plants. *Plant Physiol* 150: 786-800

Google Scholar: [Author Only](#) [Title Only](#) [Author and Title](#)

Marques-Bueno MDM, Morao AK, Cayrel A, Platre MP, Barberon M, Caillieux E, Colot V, Jaillais Y, Roudier F, Vert G (2016) A versatile Multisite Gateway-compatible promoter and transgenic line collection for cell type-specific functional genomics in *Arabidopsis*. *Plant J* 85: 320-333

Google Scholar: [Author Only](#) [Title Only](#) [Author and Title](#)

Martins S, Dohmann EM, Cayrel A, Johnson A, Fischer W, Pojer F, Satiat-Jeunemaitre B, Jaillais Y, Chory J, Geldner N, Vert G (2015) Internalization and vacuolar targeting of the brassinosteroid hormone receptor BRI1 are regulated by ubiquitination. *Nat Commun* 6: 6151

Google Scholar: [Author Only](#) [Title Only](#) [Author and Title](#)

Masalkar P, Wallace IS, Hwang JH, Roberts DM (2010) Interaction of cytosolic glutamine synthetase of soybean root nodules with the C-terminal domain of the symbiosome membrane nodulin 26 aquaglyceroporin. *J Biol Chem* 285: 23880-23888

Google Scholar: [Author Only](#) [Title Only](#) [Author and Title](#)

Morsomme P, Dambly S, Maudoux O, Boutry M (1998) Single point mutations distributed in 10 soluble and membrane regions of the *Nicotiana plumbaginifolia* plasma membrane PMA2 H<sup>+</sup>-ATPase activate the enzyme and modify the structure of the C-terminal region. *J Biol Chem* 273: 34837-34842

Google Scholar: [Author Only](#) [Title Only](#) [Author and Title](#)

Olsen RA, Clark RB, Bennett JH (1981) THE ENHANCEMENT OF SOIL FERTILITY BY PLANT-ROOTS. *American Scientist* 69: 378-384

Google Scholar: [Author Only](#) [Title Only](#) [Author and Title](#)

Pacifici E, Di Mambro R, Dello Iorio R, Costantino P, Sabatini S (2018) Acidic cell elongation drives cell differentiation in the *Arabidopsis* root. *EMBO J* 37

Google Scholar: [Author Only](#) [Title Only](#) [Author and Title](#)

Palmer CM, Guerinot ML (2009) Facing the challenges of Cu, Fe and Zn homeostasis in plants. *Nat Chem Biol* 5: 333-340

Google Scholar: [Author Only](#) [Title Only](#) [Author and Title](#)

Qi X, Zheng H (2013) Rab-A1c GTPase defines a population of the trans-Golgi network that is sensitive to endosidin1 during cytokinesis in *Arabidopsis*. *Mol Plant* 6: 847-859

Google Scholar: [Author Only](#) [Title Only](#) [Author and Title](#)

Rajniak J, Giehl RFH, Chang E, Murgia I, von Wiren N, Sattely ES (2018) Biosynthesis of redox-active metabolites in response to iron deficiency in plants. *Nat Chem Biol* 14: 442-450

Google Scholar: [Author Only](#) [Title Only](#) [Author and Title](#)

Robinson NJ, Procter CM, Connolly EL, Guerinot ML (1999) A ferric-chelate reductase for iron uptake from soils. *Nature* 397: 694-697

Google Scholar: [Author Only](#) [Title Only](#) [Author and Title](#)

Rodriguez-Celma J, Lin WD, Fu GM, Abadia J, Lopez-Millan AF, Schmidt W (2013) Mutually exclusive alterations in secondary metabolism are critical for the uptake of insoluble iron compounds by *Arabidopsis* and *Medicago truncatula*. *Plant Physiol* 162: 1473-1485

Google Scholar: [Author Only](#) [Title Only](#) [Author and Title](#)

Rogers EE, Eide DJ, Guerinot ML (2000) Altered selectivity in an *Arabidopsis* metal transporter. *Proc Natl Acad Sci U S A* 97: 12356-12360

Google Scholar: [Author Only](#) [Title Only](#) [Author and Title](#)

Santi S, Schmidt W (2009) Dissecting iron deficiency-induced proton extrusion in *Arabidopsis* roots. *New Phytol* 183: 1072-1084

Google Scholar: [Author Only](#) [Title Only](#) [Author and Title](#)

Schmid NB, Giehl RF, Doll S, Mock HP, Strehmel N, Scheel D, Kong X, Hider RC, von Wiren N (2014) Feruloyl-CoA 6'-Hydroxylase1-dependent coumarins mediate iron acquisition from alkaline substrates in *Arabidopsis*. *Plant Physiol* 164: 160-172

Google Scholar: [Author Only](#) [Title Only](#) [Author and Title](#)

Shin LJ, Lo JC, Chen GH, Callis J, Fu H, Yeh KC (2013) IRT1 degradation factor1, a ring E3 ubiquitin ligase, regulates the degradation of iron-regulated transporter1 in *Arabidopsis*. *Plant Cell* 25: 3039-3051

Google Scholar: [Author Only](#) [Title Only](#) [Author and Title](#)

Singh A, Severance S, Kaur N, Wiltsie W, Kosman DJ (2006) Assembly, activation, and trafficking of the Fet3p.Ftr1p high affinity



**iron permease complex in *Saccharomyces cerevisiae*. J Biol Chem 281: 13355-13364**

Google Scholar: [Author Only](#) [Title Only](#) [Author and Title](#)

**Tan S, Zhang P, Xiao W, Feng B, Chen LY, Li S, Li P, Zhao WZ, Qi XT, Yin LP (2018) TMD1 domain and CRAC motif determine the association and disassociation of MxlRT1 with detergent-resistant membranes. Traffic 19: 122-137**

Google Scholar: [Author Only](#) [Title Only](#) [Author and Title](#)

**Thomine S, Vert G (2013) Iron transport in plants: better be safe than sorry. Curr Opin Plant Biol 16: 322-327**

Google Scholar: [Author Only](#) [Title Only](#) [Author and Title](#)

**Vert G, Briat JF, Curie C (2001) Arabidopsis IRT2 gene encodes a root-periphery iron transporter. Plant Journal 26: 181-189**

Google Scholar: [Author Only](#) [Title Only](#) [Author and Title](#)

**Vert G, Grotz N, Dedaldechamp F, Gaymard F, Guerinot ML, Briat JF, Curie C (2002) IRT1, an Arabidopsis transporter essential for iron uptake from the soil and for plant growth. Plant Cell 14: 1223-1233**

Google Scholar: [Author Only](#) [Title Only](#) [Author and Title](#)

**von der Haar T (2007) Optimized protein extraction for quantitative proteomics of yeasts. PLoS One 2: e1078**

Google Scholar: [Author Only](#) [Title Only](#) [Author and Title](#)

**Walton A, Stes E, Cybulski N, Van Bel M, Inigo S, Durand AN, Timmerman E, Heyman J, Pauwels L, De Veylder L, Goossens A, De Smet I, Coppens F, Goormachtig S, Gevaert K (2016) It's Time for Some "Site"-Seeing: Novel Tools to Monitor the Ubiquitin Landscape in *Arabidopsis thaliana*. Plant Cell 28: 6-16**

Google Scholar: [Author Only](#) [Title Only](#) [Author and Title](#)

**Xing S, Wallmeroth N, Berendzen KW, Grefen C (2016) Techniques for the Analysis of Protein-Protein Interactions in Vivo. Plant Physiol 171: 727-758**

Google Scholar: [Author Only](#) [Title Only](#) [Author and Title](#)

**Yamada K, Nagano AJ, Nishina M, Hara-Nishimura I, Nishimura M (2013) Identification of two novel endoplasmic reticulum body-specific integral membrane proteins. Plant Physiol 161: 108-120**

Google Scholar: [Author Only](#) [Title Only](#) [Author and Title](#)

**Yi Y, Guerinot ML (1996) Genetic evidence that induction of root Fe(III) chelate reductase activity is necessary for iron uptake under iron deficiency. Plant J. 10: 835-844**

Google Scholar: [Author Only](#) [Title Only](#) [Author and Title](#)

**Yorimitsu T, Sato K, Takeuchi M (2014) Molecular mechanisms of Sar/Arf GTPases in vesicular trafficking in yeast and plants. Front Plant Sci 5: 411**

Google Scholar: [Author Only](#) [Title Only](#) [Author and Title](#)

**Yuan W, Zhang D, Song T, Xu F, Lin S, Xu W, Li Q, Zhu Y, Liang J, Zhang J (2017) Arabidopsis plasma membrane H<sup>+</sup>-ATPase genes AHA2 and AHA7 have distinct and overlapping roles in the modulation of root tip H<sup>+</sup> efflux in response to low-phosphorus stress. J Exp Bot 68: 1731-1741**

Google Scholar: [Author Only](#) [Title Only](#) [Author and Title](#)

**Yuan Y, Wu H, Wang N, Li J, Zhao W, Du J, Wang D, Ling HQ (2008) FIT interacts with AtbHLH38 and AtbHLH39 in regulating iron uptake gene expression for iron homeostasis in Arabidopsis. Cell Res 18: 385-397**

Google Scholar: [Author Only](#) [Title Only](#) [Author and Title](#)

**Zelazny E, Barberon M, Curie C, Vert G (2011) Ubiquitination of transporters at the forefront of plant nutrition. Plant Signal Behav 6: 1597-1599**

Google Scholar: [Author Only](#) [Title Only](#) [Author and Title](#)

**Zelazny E, Borst JW, Muylaert M, Batoko H, Hemminga MA, Chaumont F (2007) FRET imaging in living maize cells reveals that plasma membrane aquaporins interact to regulate their subcellular localization. Proc Natl Acad Sci U S A 104: 12359-12364**

Google Scholar: [Author Only](#) [Title Only](#) [Author and Title](#)

**Zelazny E, Miecielica U, Borst JW, Hemminga MA, Chaumont F (2009) An N-terminal diacidic motif is required for the trafficking of maize aquaporins ZmPIP2;4 and ZmPIP2;5 to the plasma membrane. Plant J 57: 346-355**

Google Scholar: [Author Only](#) [Title Only](#) [Author and Title](#)

**Zhang J, Li W, Xiang T, Liu Z, Laluk K, Ding X, Zou Y, Gao M, Zhang X, Chen S, Mengiste T, Zhang Y, Zhou JM (2010) Receptor-like cytoplasmic kinases integrate signaling from multiple plant immune receptors and are targeted by a *Pseudomonas syringae* effector. Cell Host Microbe 7: 290-301**

Google Scholar: [Author Only](#) [Title Only](#) [Author and Title](#)